mScarlet3: a brilliant and fast-maturing red fluorescent protein

Theodorus Gadella, Laura van Weeren, Jente Stouthamer, Mark Hink, Anouk Wolters, Ben Giepmans, Sylvain Aumonier, Jérôme Dupuy, Antoine Royant

1. Extended Data

Figure or Table # Please group Extended Data items by type, in sequential order. Total number of items (Figs. + Tables) must not exceed 10.	Figure/Table title One sentence only	Filename Whole original file name including extension. i.e.: Smith_ED_Fig1.jpg	Figure/Table Legend If you are citing a reference for the first time in these legends, please include all new references in the main text Methods References section, and carry on the numbering from the main References section of the paper. If your paper does not have a Methods section, include all new references at the end of the main Reference list.
Extended Data Table. 1	**Properties of red fluorescent proteins**	Gadella_ED_Table1.pdf	[a]Absorbance maximum. [b]Emission maximum. [c]Extinction coefficient at maximum absorbance. [d]Quantum yield. [e]Fluorescence lifetime component 1. [f]Fluorescence lifetime component 2. [g]Amplitude of fluorescence lifetime component 1. [h]Chi-square fluorescence lifetime fit. [i]Average fluorescence lifetime weighed by amplitude. [j]Modulation lifetime in cells. [k]Apparent p*K*a value. [l]Hill coefficient. [m]Calculated intrinsic brightness, product of extinction coefficient and quantum yield. [n]Brightness in mammalian cells normalized to mScarlet-I. [o]Time in seconds to half the emission rate under wide field conditions. [p]Time in seconds to half the emission rate under confocal spinning disk conditions. [q]Percentage of photochromic behavior. [r]Accumulation in cells normalized to mScarlet-I (brightness in cells divided by intrinsic brightness). [s]Apparent delay time of maturation relative to mTurquoise2 in mammalian cells. [t]Initial fluorescence at pH 13.5 relative to pH 7.4. [u]Time required to reduce fluorescence by 50% at pH 13.5. Sensitized emission by FRET in a RFP-SYFP2 fusion, corrected for direct excitation of donor and acceptor, normalized to mScarlet-I. [w]Percentage of cells with a correct ER labelling upon expressing an Cyterm-RFP fusion. [x]Percentage of cells visible OSER structures upon expressing an Cyterm-RFP fusion . [y]Number of analyzed cells. [z] Values from Semiakina et al..

			c,d,e,f,j,k,n,m,n,q,r,s ± standard deviation, or value cited from literature. Values in *Italics* from Bindels et al., 2016.
Extended Data Fig. 1	**Brightness of RFPs in HeLa cells 24 h after transfection**	Gadella_ED_fig1.pdf	For each RFP an mTurquoise2 construct was coexpressed in cells in a 1:1 molecular ratio. The average red fluorescence and cyan fluorescence was quantified for each cell (red data points). a mScarlet3 n=231, b mScarlet-I3 n=303, c mScarlet n=238, d mApple n=266, e mCherry n=272, f mScarlet-I n=303, g mKate2 n=294, h mRuby3 n=275, I FusionRed n=156, j TagRFP-T n=320, and k dTomato n=268. The red fluorescence values were corrected for spectral throughput of the microscope (correcting for instrument-dependent excitation and detection efficiencies of the different RFPs). The slopes of the linear regression line that is forced the origin was used for calculating the relative brightness of the RFPs (as compared to mScarlet) and indicated in Extended Data Table I and Fig. 1d. The slope was calculated as $\sum RC/\sum C^2$ in which R is the RFP intensity value of a single cell (vertical axes) and C is the CFP intensity of the same cell (horizontal axes). The standard error of the slope (indicated in Fig. 1d and Extended Data Table 1) was calculated as $Sqrt((\sum R^2-(\sum RC)^2/\sum C^2)/((n-1)\sum C^2))$. In which n is the number of cells.
Extended Data Fig. 2	**Alkaline denaturation speed of diverse purified RFPs at pH 13.5**.	Gadella_ED_fig2.pdf	**a**: logarithmic time axis, **b**: normal time axis.
Extended Data Fig. 3	**Photostability of RFP variants**	Gadella_ED_fig3.pdf	**a**: Widefield bleaching of mScarlet variants without time-axis correction, **b**: same data as a) but y-axis scaled according to cellular brightness; **c**: confocal bleaching of

			mScarlet variants; **d**: confocal bleaching of mScarlet variants and other RFPs. In order to fairly compare the photostability of different RFP variants under confocal imaging conditions, the time axis is corrected in c and d for spectral properties relative to mScarlet to mimic an identical overall emission rate (photons/s) for all RFPs at the start of the experiment. **e**: Blue light-induced photochromicity of RFP variants. The RFP variants were expressed in HeLa cells and continuously exposed with 550 nm excitation light. At t=15, 31, 46 and 52 s, the 550 nm excitation light interrupted by a brief excitation at 470 nm for 1 s (not recorded on time axis) after which the 550 nm excitation was continued. The sudden increase after blue light excitation is caused by photochromic behavior.
Extended Data Fig. 4	**Evaluation of RFPs as fusion tag in HeLa cells**	Gadella_ED_fig4.pdf	**a-h**: representative images of selected Cyterm-RFP fusions in HeLa cells 24h after transfection. **a** FusionRed, **b** mScarlet3; **c** TagRFP-T; **d** mCherry; **e** mScarlet-I3; **f** mScarlet-I3-NCwt; **g** mScarlet-I; **h** mScarlet. For a-h bar is 10 µm and the fluorescence intensities were pseudo-colored between minimum and maximum intensities according to the mScarlet lookup table as indicated in image d and subsequently gamma-corrected (value 0.5, including the lookup table) to better visualize the low intensity areas. For cell numbers imaged and evaluated see Extended data Table 1, images shown are representative of these. **I-l**: mScarlet3 as fusion tag for cellular localization studies. mScarlet3 was fused to: **i** alpha-tubulin (microtubule cytoskeleton); **j** EB3 (+ends of microtubules); **k** Giantin (Golgi apparatus); and **l** a 3x

			repeated nuclear localization signal (NLS) (nuclei) and expressed in HeLa cells. For i-l bar is 10 µm and the fluorescence intensity was pseudo-colored between minimum and maximum fluorescence according to the mScarlet lookup table indicated in l. Micrographs shown in i-l are representative of at least 4 images made from 2 independent transfections.
Extended Data Fig. 5	**FRET in HeLa cells expressing SYFP2 alone or SYFP2-RFP fusion proteins**	Gadella_ED_fig5.pdf	**. a.** Average FRET spectra from HeLa cells expressing SYFP2 alone or SYFP2-RFP fusion proteins. All spectra were normalized to the unquenched SYFP2 donor. **b**. Quantification of FRET spectra from a. E (blue bars) represent the energy transfer efficiency (average ± sd), and Qs (red bars) depict the sensitized emission quantum yield (average ± sd). Qs is defined as the number of sensitized emission quanta emitted by the RFP acceptor divided by the number of quanta absorbed by the SYFP2 donor and is calculated by Qs=E·Qa, in which Qa is the acceptor quantum yield of fluorescence. Qs is not dependent on the emission spectra and is proportional to the integrated acceptor sensitized emission signal. Each data point represents quantitative unmixing analysis of a single cell spectrum, 18-25 single cell spectra were recorded for each condition. **c**. SYFP2 fluorescence lifetime of HeLa cells expressing SYFP2 alone or SYFP2-RFP fusion proteins as determined by frequency-domain FLIM. Tau(phi) (red bars) is the average lifetime estimated from the phase shift (± sd), Tau(mod) (blue bars) is the average fluorescence lifetime estimated from the demodulation (± sd). For c each data point represents the average lifetime of an image with 4-

			20 individual cells, 4-6 FLIM recordings were done for each condition.
Extended Data Fig. 6	**Relative cell viability of RFP transfected cells**	Gadella_ED_fig6.pdf	mEGFP and RFPs were transfected separately into HeLa cells at day 0. At day 2 each of the RFP transfected cells were split and mixed with mEGFP transfected cells. At days 4 and 6 the cell mixtures were resplit. At days 2, 4 and 6 after (4-5 h after splitting/mixing) the number of RFP and mEGFP expressing cells in the mixtures was scored. The ratio of RFP to mEGFP expressing cells was normalized to that obtained at day 2 to correct for bias in transfection efficiencies. For each RFP 8-12 technical replicates (depicted as individual data points) were measured. The average normalized ratio of red to green cell numbers ± sd is indicated.
Extended Data Fig. 7	**Brightness of RFPs in mammalian cells after fixation relative to mScarlet**	Gadella_ED_fig7.pdf	Indicated is the average relative brightness (± sd), corrected for spectral throughput determined from single cell red to cyan ratios and linear regression (though the origin) like in Extended Data Fig. 1.
Extended Data Fig. 8	**Illustration of the potential van der Waals interactions between 9 residues of mScarlet3 near the surface of the one face of the β-barrel**	Gadella_ED_fig8.pdf	Residues belong to the central α-helix traversing the β-barrel (Thr74), to the α-helix capping one head of the β-barrel (Trp84), to the loop linking the latter helices (His76), to the 7th strand (Leu151), to the 8th strand (Leu158), to the loop bridging the 9th and 10th strands (Pro191), to the 10th strand (Phe194, Ile196), to the 11th strand (Ala220). Potential van der Waals interactions (dashed black lines) are highlighted by inter-carbon atom distances below 4.0 Å. **a**. View from the side of the β-barrel. The set of vdW interactions forms a crown-like structure.**b**. 90° view (from the barrel head) showing residues organized in three layers: the main one is

			formed of residues Thr74, Trp84, Leu158, Phe194 and Ala220, with residues His65 and Pro191 ahead of this layer, and residues Leu151 and Ile196 behind it.
Extended Data Fig. 9	**Evolution path for mScarlet3 (seq-id #15) and mScarlet-I3 (#16) from mScarlet (#1) and mScarlet-I (#2), respectively**	Gadella_ED_fig9.pdf	The numbers correspond with the sequence IDs in Extended Data Table 2. The horizontal axis depicts the (modulation) fluorescence lifetime as determined in live HeLa cells ~ 24 h after transfection and corresponds with intrinsic brightness (more to the right is better), and the vertical axis depicts the cellular brightness (higher is better) normalized to mScarlet-I. F. Vertical error bars are SD of the slope of the line fitted to the red to cyan cellular ratios (of 22-77 cells, e.g. see Extended Data Fig. 1) or the average modulation lifetime of the mScarlet variant in HeLa cells (from 3 individual FLIM recordings with > 5 cells each)

1. Supplementary Information:

A. PDF Files

Item	Present?	Filename Whole original file name including extension. i.e.: Smith_SI.pdf. The extension must be .pdf	A brief, numerical description of file contents. i.e.: *Supplementary Figures 1-4, Supplementary Discussion, and Supplementary Tables 1-4.*
Supplementary Information	YES	Gadella_SI.pdf	Supplementary notes, references, Figure, Tables and movie legends

Reporting Summary	Yes	NMETH-BC49688Breportingsumm.pdf
Peer Review Information	No	*OFFICE USE ONLY*

B. Additional Supplementary Files

Type	Number Each type of file (Table, Video, etc.) should be numbered from 1 onwards. Multiple files of the same type should be listed in sequence, i.e.: Supplementary Video 1, Supplementary Video 2, etc.	Filename Whole original file name including extension. i.e.: *Smith_ Supplementary_Video_1.mov*	Legend or Descriptive Caption Describe the contents of the file
Supplementary Video	Supplementary Video 1	Gadella_Supplementary_Video_1.avi	**Confocal timelapse of mScarlet3-Cyterm imaged in U2Os cells 48 h after transfection.** In addition to ER and nuclear envelope labelling also motile punctate endomembrane structures appear that are possibly involved in removal of mScarlet3-Cyterm from the ER. This is particularly apparent in the top right cell. Total Video duration 42 s at 0.32 s frame rate
Supplementary Video	Supplementary Video 2	Gadella_Supplementary_Video_2.avi	**Prolonged confocal imaging of actin dynamics using Lifeact-mScarlet3.** Actin dynamics was imaged in HeLa cells transfected with pLifeact-mScarlet3. 1000 frames were captured each with 2

			scans averaged. No noticeable bleaching is observed. Total Video duration is 16 h at 1 min frame rate.
Supplementary Video	Supplementary Video 3	Gadella_Supplementary_Video_3.avi	**Microtubule polymerization visualized by EB3-mScarlet3 in HeLa cells.** Total Video duration is 2 minutes in real time, bar is 10 µm.
Supplementary Video	Supplementary Video 4	Gadella_Supplementary_Video_4.avi	**Dynamic microtubules visualized by expression of mScarlet3-alpha tubulin in HeLa cells.** Total Video duration is 2 minutes in real time, bar is 10 µm.
Supplementary Video	Supplementary Video 5	Gadella_Supplementary_Video_5.avi	**mScarlet3 applied for prolonged live-cell imaging of nuclei in pancreatic cells in zebrafish larvae.** H2A-mScarlet3 was expressed under an elastase promotor and examined on a light sheet microscope. Nuclear localization is found only in the exocrine cells of the pancreas. Movement is caused by motion of the larva. Total Video duration of 12 h in real time at 15 min frame rate.
Supplementary Video	Supplementary Video 6	Gadella_Supplementary_Video_6.avi	**Lightsheet microscopy of H2B-mScarlet3 labelled cell nuclei in a developing zebrafish larva – full larva.** Total duration 355 min.
Supplementary Video	Supplementary Video 7	Gadella_Supplementary_Video_7.avi	**Lightsheet microscopy of H2B-mScarlet3 labelled cell nuclei in a developing zebrafish larva - zoom on mitotic cells.** Total duration 355 min (zoom). Note several dividing cells.

3. Source Data

Parent Figure or Table	Filename Whole original file name including extension. i.e.: *Smith_SourceData_Fig1.xls,* or *Smith_ Unmodified_Gels_Fig1.pdf*	Data description i.e.: Unprocessed western Blots and/or gels, Statistical Source Data, etc.
Source data Fig. 1	Gadella_source_data_Fig1.xlsx	Source data for Fig 1a-i
Source data Fig. 2	Gadella_source_data_Fig2.xlsx	Source data for Fig 2i
Source data ED Fig. 1	Gadella_source_data_ED_Fig1.xlsx	Source data for extended data Fig 1
Source data ED Fig. 2	Gadella_source_data_ED_Fig2.xlsx	Source data for extended data Fig 2a,b
Source data ED Fig. 3	Gadella_source_data_ED_Fig3.xlsx	Source data for extended data Fig 2a,b
Source data ED Fig. 5	Gadella_source_data_ED_Fig5.xlsx	Source data for extended data Fig 3a-e
Source data ED Fig. 6	Gadella_source_data_ED_Fig6.xlsx	Source data for extended data Fig 5a-c
Source data ED Fig. 7	Gadella_source_data_ED_Fig7.xlsx	Source data for extended data Fig 7
Source data ED Fig. 9	Gadella_source_data_ED_Fig9.xlsx	Source data for extended data Fig 9

mScarlet3: a brilliant and fast maturing red fluorescent protein

Theodorus W.J. Gadella Jr[1*], Laura van Weeren[1], Jente Stouthamer[1], Mark A. Hink[1], Anouk H.G. Wolters[2], Ben N.G. Giepmans[2], Sylvain Aumonier[3], Jérôme Dupuy[3], Antoine Royant[3,4]

[1]Section of Molecular Cytology and van Leeuwenhoek Centre for Advanced Microscopy, Swammerdam Institute for Life Sciences, University of Amsterdam, Amsterdam, the Netherlands.

[2]Biomedical Sciences of Cells & Systems, University of Groningen UMC Groningen, The Netherlands

[3]Univ. Grenoble Alpes, CNRS, CEA, Institut de Biologie Structurale, Grenoble, France.

[4]European Synchrotron Radiation Facility, Grenoble, France.

* Correspondence should be addressed to T.W.J.G. (th.w.j.gadella@uva.nl)

We report the evolution of mScarlet3, a cysteine-free monomeric red fluorescent protein with fast and complete maturation, record brightness, -quantum yield (75%) and -fluorescence lifetime (4.0 ns). The mScarlet3 crystal structure reveals a barrel rigidified at one of his heads by a large hydrophobic patch of internal residues. mScarlet3 behaves well as fusion tag, displays no apparent cytotoxicity and it surpasses existing red fluorescent proteins as Förster resonance energy transfer (FRET) acceptor and as reporter in transient expression systems.

Red fluorescent proteins (RFPs) found in Anthozoa species[1] are structurally related to GFP found in *Aequoria victori*a and fold in highly similar yet tetrameric beta-barrel structures[2]. Much effort has been devoted to monomerize RFPs. After the first, relatively dim, mRFP1 was described[3], other brighter variants were created as mCherry[4], TagRFP[5], mRuby3[6], mKate2[7]

and FusionRed[8]. However, irrespective of improvements, all of these second generation mRFPs still suffer from relatively low quantum yield, photochromicity or residual dimerization tendency. For this reason, we developed the mScarlet series of RFPs[9]. mScarlet displays the highest intrinsic brightness (multiplication of extinction coefficient and quantum yield), no photochromicity and is monomeric, but its maturation is relatively slow. mScarlet-I with lower intrinsic brightness is brighter in cells owing to faster and more complete maturation. Interestingly, in a recent study mCherry-XL with an equal fluorescence quantum yield (70%) as mScarlet was evolved, but owing to reduced maturation, the brightness in cells was half of mScarlet[10]. Obviously, a variant combining fast maturation and the highest possible intrinsic brightness is highly desirable. For instance, for building FRET sensors with an RFP acceptor, the extent of RFP maturation defines the extent of donor quenching, whereas its intrinsic brightness determines the intensity of the sensitized emission, both contributing to high FRET contrast.

Because random mutagenesis to create brighter mScarlet variants proved unsuccessful [9], we devised a targeted approach towards amino acids surrounding Threonine-74, since this is the only mutated amino acid in mScarlet-I as compared to mScarlet. With multiparameter screening[11], we evolved variants of mScarlet-I with a higher quantum yield and variants of mScarlet with faster maturation (see Supplementary note 1).

After several rounds of targeted and random mutagenesis we generated two final variants mScarlet-3 and mScarlet-I3 (for spectra see Fig. 1a and b). Spectroscopic evaluation of purified mScarlet3 (Extended Data Table I) revealed that it has a quantum yield of 75%, and extinction coefficient of 104,000 M^{-1} cm^{-1} and it displays a long monoexponential fluorescence lifetime of 4.0 ns (Fig. 1c). Spectroscopic analysis of mScarlet-I3 revealed a seriously enhanced quantum yield (65%) and an 21% increased intrinsic brightness as compared to mScarlet-I, approaching that of mScarlet (95%) (Extended Data Table I). Intrinsic brightness of purified FPs, however, does not always report on the actual brightness found in cells, since the latter additionally depends on the extent and speed of chromophore maturation. Importantly, in cells, mScarlet3 and mScarlet-I3 are 76% and 80% brighter as compared to mScarlet and > 5-fold brighter than mCherry, owing to a substantially faster and more complete maturation (Extended Data Table I, Fig. 1d, Extended Data Fig. 1). By directly comparing the intrinsic brightness with the cellular brightness, one can infer the overall extent of maturation. It was found that after 24 h mScarlet3 matures to an equal extent (96%) as the very efficiently

maturing mScarlet-I (Fig. 1e). mScarlet-I3 maturation is more complete (113%) than mScarlet-I. mScarlet3 matures 4 times faster than mScarlet and equally fast as mCherry (Extended Data Table I, Fig. 1f). mScarlet-I3 is the fastest maturing monomeric RFP tested. Surprisingly, in alkaline denaturation experiments, we found a marked stability of mScarlet3: where mScarlet and mScarlet-I denaturate instantaneously (< 1 s) at pH 13.5, mScarlet3 retained more than half of its initial fluorescence for over 40 minutes (Extended Data Fig. 2). mScarlet3 (pKa=4.5) and mScarlet-I3 (pKa=4.2) have better acid resistance as compared to mScarlet(-I) (pKa=5.4), which would be beneficial for applications of these RFPs in endomembrane studies (Fig. 1g, Supplementary Video 1). At high excitation power, the photobleaching kinetics are slightly faster as compared to the precursors, with mScarlet3 performing better in confocal bleaching (see Extended Data Table I, Extended Data Fig. 3a-d). Notwithstanding, mScarlet3 is photostable enough to permit 1000 confocal scans under live cell confocal timelapse imaging conditions without noticeable photobleaching (Supplementary Video 2). We also tested photochromicity in alternating blue and green excitation and we found that both mScarlet3 and mScarlet-I3 are non-photochromic (like mScarlet, mScarlet-I and mCherry) (Extended Data Table I, Extended Data Fig. 3e), which is in great contrast to mApple, mRuby3, TagRFP-T and FusionRed[9,12]. mKate2 and TagRFP-T showed increased red fluorescence after several photochromic cycles (Extended Data Fig 3d,e). Photochromic behavior can be highly problematic in quantitative ratiometric FRET studies[9]. mScarlet3 and mScarlet-I3 display monoexponential fluorescence decay with long lifetimes of 4.0 and 3.6 ns, respectively, facilitating possible application as donors in FRET-FLIM.

Since both mScarlet3 and mScarlet-I3 contain new N and C termini and various mutations on the exterior of the beta-barrel (see Supplementary note 1, Supplementary Fig. 1), we performed an OSER (organized smooth ER) assay to address their monomeric behavior[13]. Indeed, the OSER test revealed no enhanced oligomerization (Extended Data Table 1, Extended Data Fig. 4a-h).

Several fusion constructs with mScarlet3 to label specific cellular organelles and structures were made. In all instances bright labelling of the correct structures and localizations was found (Fig. 2a-f, Extended Data Fig. 4 i-l, Supplementary Video 3). Also, the direct fusion to alpha-tubulin, which is known to be very adversely affected by residual dimerization tendency of FPs, revealed nice microtubular structures displaying dynamic instability [14](Supplementary Video 4).

The new mScarlets are superior FRET acceptors of a monomeric yellow fluorescent protein SYFP2: in ratiometric spectral FRET, mScarlet3 quenches SYFP2 fluorescence intensity as efficiently as mScarlet-I (both 53%) and better than mCherry (46%) or mScarlet (37%) (Fig. 1h & Extended Data Figs 5a,b). The yield in sensitized emission is substantially improved for mScarlet3 (140% as compared to mScarlet-I, 154% as compared to mScarlet and 377 % as compared to mCherry). The better quenching of SYFP2 is also seen by FLIM analysis of the τ_{φ} fluorescence lifetime of SYFP2 that is more reduced with mScarlet3 (1.67 ns) than with mScarlet (1.85 ns) or mCherry (1.77 ns) (Extended Data Fig. 5c). We found a small negative effect of the new N and C termini on FRET levels, possibly due to another average orientation despite our efforts in keeping the linker length identical in the comparison of the diverse fusions (see Extended Data Table 1, Extended Data Fig. 5). Although mScarlet-I3 seems to be a slightly better quencher of SYFP2 than mScarlet3, it produces less sensitized emission due to its lower quantum yield. Hence, mScarlet3 is the best FRET acceptor of yellow fluorescent proteins, providing equal YFP quenching but 40% more sensitized red emission as compared to mScarlet-I (the previously best performing RFP).

Because mScarlet3 and mScarlet-I3 incorporate the new C and N termini originally described for mScarlet-I2[15] for which it was shown to reduce cytotoxicity in bacteria, we tested for cytotoxicity in mammalian cells. Within 48 h after transfection, we found no apparent cytotoxicity of mScarlet3 or mScarlet-I3 expression (Fig. 1i). By monitoring fluorescently labeled cells at 4 and 6 days after transfection, we found slightly more cells producing mScarlet-I3 or mScarlet3 as compared to other RFPs (Extended Data Fig. 6), also suggesting no apparent cytotoxicity. We tested the resistance to paraformaldehyde fixation, where mScarlet3 proved to be the brightest RFP variant after fixation (Extended Data Fig. 7).

To understand the structural basis for the improvements found in mScarlet3, we determined its crystal structure at physiological pH at 1.33 Å resolution (see online Methods and Supplementary Note 2). The conformations of the chromophore and its surrounding residues (first coordination sphere) are perfectly superimposable on those observed in the pH 7.8 crystal structure of mScarlet[9]. Yet, the key residue Glu216 adopts two alternate conformations, like in the bright green FP EGFP (Fig. 2g). We focused our analysis on the mutations within the bulk of the protein barrel: Y84W, Y194F, V196I, and G220A. Coincidentally, these four mutations remove two polar atoms and add six non-polar atoms, which results in the replacement of a small amphipathic cavity by a hydrophobic patch purely

involving methyl or methine carbon atoms (Fig. 2h). This hydrophobic patch is linking together the tips of 4 of the 11 beta-strands of the protein and of the chromophore-bearing alpha-helix, as well as a loop and a helix bridging pairs of strands (Extended Data Fig. 8). Thereby it contributes to the increased rigidification of one head of the beta-barrel and the increased fluorescence QY of mScarlet3.

To assess the performance of mScarlet3 for *in vivo* applications, we first compared mScarlet and mScarlet3 for brightness in zebrafish larvae. 24 h after injection of plasmid, a 2-fold increased red fluorescence was detected for mScarlet3 in larvae (Fig. 2i), in good agreement with the values found in mammalian cells (Fig. 1d, Extended Data Figs. 1, 7). Additionally, injections were made of H2B-mScarlet3 produced in exocrine cells of the pancreas (Fig. 2j; Supplementary Video 5). Finally, we imaged H2B-mScarlet3 for 6 hours in 5 min intervals (z-stack of 309 frames) in all cells in zebrafish larvae following mRNA injection and found many cells going through mitosis (Fig. 2k, Supplementary Video 6 and 7). Thus, mScarlet3 is useful for *in vivo* examination of cells in zebrafish larvae.

In conclusion, we have evolved a brilliant new red fluorescent protein mScarlet3 that uniquely combines the highest quantum yield of RFPs, monomeric behavior, no apparent cytotoxicity and absence of photochromic behavior with fast and complete maturation (Extended Data Fig. 9). In all tested fusions, mScarlet3 demonstrated excellent performance as fusion-tag, as FRET acceptor and in live cell applications. While chromophore rigidity is essential for high quantum yield, too much rigidity may hamper FP maturation that requires a certain degree of internal flexibility to assist fast kinetics of chromophore formation and -oxidation. We speculate that the engineered hydrophobic patch (Fig. 2h) exactly does that job. We do not exclude that other existing bright FPs can be still improved to combine maximal brightness and maturation by following the same recipe of multiparameter (at least brightness and fluorescence lifetime) screening[11].

Acknowledgments

We are grateful to Ronald Breedijk (Amsterdam) for his assistance and the maintenance of the LCAM microscopes and to Sylvain Engilberge (Grenoble) for his assistance in drawing mScarlet3 structural figures. Part of the work has been performed in the UMCG Microscopy and Imaging Center (UMIC). This work was supported by a grant from the French Agence Nationale de la Recherche (ANR-17-CE11-0013 to J.D.).

175

176 **Author contributions**

177 TWJG designed and supervised the project. LvW & JS performed the mutagenesis
178 experiments. LvW prepared bacteria, purified proteins, cultured and transfected mammalian
179 cells. TWJG performed and analyzed the spectroscopic characterization and cellular imaging
180 experiments. MAH performed and analyzed the TCSPC experiments. AHGW and BNGG
181 performed and analyzed the zebrafish experiments. SA, JD and AR purified mScarlet3 for
182 crystallization, crystallized mScarlet3 and solved and analyzed the crystal structure. TWJG and
183 AR wrote the manuscript with input from all authors.

184

185 **Competing interests**

186 The University of Amsterdam has applied for a European Patent (EP 33108) and international
187 PCT Patent (WO 35192) (patents pending) on "Improved variants of monomeric scarlet red
188 fluorescent protein" with TWJ Gadella and L van Weeren as inventors. Otherwise, the authors
189 declare no competing interests.

190

191 **Figure Legends**

192 **Fig. 1. Characterization of mScarlet3 and mScarlet-I3.** Normalized absorbance, excitation,
193 and emission spectra of mScarlet3 (**a**) and mScarlet-I3 (**b**). For the fluorescence excitation
194 spectra, the emission was set at 620 nm, for the fluorescence emission spectrum excitation
195 was set at 540 nm. **c**. Fluorescence decay of mScarlet3 fitted with a single exponential
196 lifetime of 3.96 ns. The weighted residuals show a perfect fit (χ^2=1.18). **d**. Relative
197 brightness (average ± sd) of RFPs in HeLa cells24 h after transfection, determined by
198 normalized, spectrally-corrected ratios of red to cyan fluorescence intensity found in cells
199 upon co-production of RFP and mTurquoise2 (See Extended Data Fig. 1). **e**. Maturation
200 extent of RFPs in HeLa cells relative to mScarlet-I (average ± sd) 24 h after transfection
201 calculated by dividing the cellular brightness (Fig 1d) by the intrinsic brightness (Extended
202 Data Table 1). **f**. Maturation speed of RFPs in mammalian cells measured as delay (average ±
203 sd in h) relative to co-produced mTurquoise2, n=7-10 cells. **g**. pH dependence of the
204 fluorescence intensity of mScarlet3, mScarlet-I3 and mScarlet. **h**. Spectral analysis of FRET
205 between SYFP2 and diverse RFPs in living HeLa cells. All spectra are corrected for detector
206 sensitivity and normalized to the unquenched SYFP2 signal. **i**. Check for cytotoxicity of

fluorescent protein expression in HeLa cells 48 h after transfection quantified by NAD(P)H/live cell-dependent conversion of WST-8 into blue light absorbing formazan (average absorbance at 460 nm ± sd for each 6 independent transfections).

Fig. 2. Characterization of the cellular and in vivo applications of mScarlet3 and of the mScarlet crystal structure. a-f usage of mScarlet3 as fusion tag in HeLa cells, bar=10 µm, red fluorescence intensity was scaled according to the mScarlet LUT (in a) micrographs are representative of at least 4 images in 2 independent transfections. Cells were producing ER-mScarlet3 (**a**, endoplasmic reticulum), LaminB-mScarlet3 (**b**, nuclear envelope); 4xmito-mScarlet3 (**c**, mitochondria); lifeact-mScarlet3 (**d**, actin cytoskeleton); mScarlet3-peroxi (**e**, peroxisomes); and LCK-mScarlet3 (**f**, plasma membrane). **g**. Alternate conformations of Glu216 in mScarlet3. $2F_{obs}$ - F_{calc} electron density map contoured at a 1.5 σ level and superimposed on the chromophore and the surrounding residues Arg198 and Glu216. Glu216 unambiguously exhibits two distinct conformations of its side chain, leading to the positioning of one water molecule in alternate conformations. **h**. Comparison of a region near one head of the beta-barrel between mScarlet (blue) and mScarlet3 (magenta), showing how the concerted mutations of four residues lead to the formation of a hydrophobic patch. Arrows indicate the additional non-polar atoms introduced in mScarlet3 contributing to both the volume decrease of a small amphipathic cavity and the increase in the number of potential van der Waals interactions. **i**. Brightness of mScarlet (green symbols) and mScarlet3 (red symbols) in fixed zebrafish larvae 24h post injection. Points represent measurements of average fluorescence intensity found in confocal pictures of individual cells relative to a coproduced mTurquoise2, lines represent linear regression through the origin. **j**. mScarlet3 applied for live-cell imaging of pancreatic cells in zebrafish. H2B-mScarlet3 was expressed under an elastase promotor and examined on a light sheet microscope. Nuclear localization is found in the exocrine cells of the pancreas. Note the cell division in the boxed area. Bar: 5 µm. **k** Lightsheet microscopy of H2B-mScarlet3 labelled cell nuclei in a developing zebrafish larva (see also corresponding Supplementary Video 6).

References

1. Matz, M. V. *et al.* Fluorescent proteins from nonbioluminescent Anthozoa species. *Nat Biotechnol* **17**, 969–973 (1999).
2. Yarbrough, D., Wachter, R. M., Kallio, K., Matz, M. v. & Remington, S. J. Refined crystal structure of DsRed, a red fluorescent protein from coral, at 2.0-Å resolution. *Proc Natl Acad Sci U S A* **98**, 462–467 (2001).
3. Campbell, R. E. *et al.* A monomeric red fluorescent protein. *Proc Natl Acad Sci U S A* **99**, 7877–7882 (2002).
4. Shaner, N. C. *et al.* Improved monomeric red, orange and yellow fluorescent proteins derived from Discosoma sp. red fluorescent protein. *Nat Biotechnol* **22**, 1567–1572 (2004).
5. Merzlyak, E. M. *et al.* Bright monomeric red fluorescent protein with an extended fluorescence lifetime. *Nat Methods* **4**, 555–557 (2007).
6. Bajar, B. T. *et al.* Improving brightness and photostability of green and red fluorescent proteins for live cell imaging and FRET reporting. *Sci Rep* **6**, 20889 (2016).
7. Shcherbo, D. *et al.* Far-red fluorescent tags for protein imaging in living tissues. *Biochemical Journal* **418**, 567–574 (2009).
8. Shemiakina, I. I. *et al.* A monomeric red fluorescent protein with low cytotoxicity. *Nat Commun* **3**, 1204 (2012).
9. Bindels, D. S. *et al.* MScarlet: A bright monomeric red fluorescent protein for cellular imaging. *Nat Methods* **14**, 53–56 (2017).
10. Mukherjee, S. *et al.* Directed Evolution of a Bright Variant of mCherry: Suppression of Nonradiative Decay by Fluorescence Lifetime Selections. *Journal of Physical Chemistry B* **126**, 4659–4668 (2022).
11. Bindels, D. S., Postma, M., Haarbosch, L., van Weeren, L. & Gadella, T. W. J. Multiparameter screening method for developing optimized red-fluorescent proteins. *Nat Protoc* **15**, 450–478 (2020).
12. Shaner, N. C. *et al.* Improving the photostability of bright monomeric orange and red fluorescent proteins. *Nat Methods* **5**, 545–551 (2008).

13. Costantini, L. M., Fossati, M., Francolini, M. & Snapp, E. L. Assessing the Tendency of Fluorescent Proteins to Oligomerize Under Physiologic Conditions. *Traffic* **13**, 643–649 (2012).
14. Costantini, L. M. *et al.* A palette of fluorescent proteins optimized for diverse cellular environments. *Nat Commun* **6**, 1–13 (2015).
15. Valbuena, F. M. *et al.* A photostable monomeric superfolder green fluorescent protein. *Traffic* **21**, 534–544 (2020).

Online Methods:

General Methods

All red fluorescent proteins (RFPs) were cloned into a pDRESS plasmid (Addgene 130509) [11] or pDX vector (a modified TriEX vector, expressing a FP in both bacteria, under a rhamnose promoter, and in mammalian cells, under a CMV promoter) using the AgeI and BsrGI restriction sites. mRuby3 [6], TagRFP-T [12], mApple [12], mCherry [4] mKate2 [7] and FusionRed [8] were obtained as described in [9]. The new vectors pDRESS_mTurquoise2_spatial-linker-P2A_mScarlet3 (189752, Addgene), pDx_mScarlet3 (189754, Addgene), pDRESS_mTurquoise2_spatial-linker-P2A_mScarlet-I3 (189755, Addgene), pDx_mScarlet-I3 (189757, Addgene) were deposited at Addgene. Mammalian cell imaging was done with U2OS cells (HTB-96, ATCC) or HeLa cells (CCL-2 ATCC). Mammalian cells were grown in 24 well plates with glass bottom (MatTek P24G-1.5-13-F) in DMEM (61965059, Thermo Fisher Scientific) containing 10% fetal bovine serum (10270106, Thermo Fisher Scientific) or with colorless DMEM 11594416 Thermo Fisher Scientific) supplemented with 1% of Glutamax (11574466 Thermo Fisher Scientific) under 7% humidified CO2 atmosphere at 37 °C. For transfection polyethylenimine (PEI) in ddH2O (1 mg/ml, pH 7.3, 23966, Polysciences) was used. The transfection mixture was prepared in Opti-MEM (31985047, Thermo Fisher Scientific) with 2 µl PEI solution and 50-200 ng plasmid. For some transfections, carrier DNA (empty plasmid) was added to prevent overexpression. The transfection mixture was incubated for 20–45 min. Cells were used for imaging 15-48 h after transfection.

Mutagenesis

mScarlet variants were obtained by site-directed and random mutagenesis using standard protocols, see [9]. Evolution started from mScarlet and mScarlet-I by introducing G220A (Seq-ID 3,4 (see Supplementary Fig 1)), followed by V196I (Seq-ID 5,6) targeted mutagenesis. With random mutagenesis the combination of T107S, G156V and E219V was found to be beneficial. A new template mScarlet-2A (Seq-ID 7) was ordered as geneblock carrying T107S, G156V, V196I, E219V and G220A as mutations relative to mScarlet. T74I was introduced into mScarlet-2A to yield mScarlet-2A-I (Seq-ID 8). Y84W was introduced in mScarlet-2A by targeted mutagenesis, yielding mScarlet-2A-84W (Seq-ID 9). We also introduced T74I into mScarlet-2A-84W to yield mScarlet-I-2A-84W (Seq-ID 10). These two new templates were

subjected to an additional round of random mutagenesis. From screening of several variants of mScarlet-2A-84W were found with increased maturation, one with two mutations T109A, K183R, one with the single mutation Y194F and one with the single mutation K48R with increased brightness. We first combined T109A, K183R and Y194F, yielding mScarlet-2A-84W-R8-194F (Seq-ID 11). Introducing K48R yielded a slight further brightness increase in mScarlet3-NCwt (Seq-ID 13). With PCR new N and C termini [15] were introduced (Δ1, V2M, S3D, K4S, G5T and M227S, D228G, E229G, S230S, Δ231, Δ232) yielding mScarlet3 (Seq-ID 15). In the random mutagenesis of mScarlet-2A-I-84W a combination of 6 mutations originating from different mutated variants were found to be beneficial. These mutations were introduced by ordering a new template mScarlet-I-2A-84W-nt1 (Seq-ID 12) containing K93R, N99I, A105T, T128G, K140R, Y194F relative to the mScarlet-2A-I-84W template. Subsequent scrutinizing demonstrated that reversal of R93K by targeted mutagenesis was beneficial yielding mScarlet-I3-NCwt (Seq-ID 14). With PCR new N and C termini were introduced (Δ1, V2M, S3D, K4S, G5T and M227S, D228G, E229G, S230S, Δ231, Δ232) yielding mScarlet-I3 (Seq-ID 16).

Protein purification

His-tagged recombinant RFPs were purified from E coli bacteria as described [9] except for the final affinity purification and dialysis steps. For affinity purification the crude E coli protein extract was obtained from defrosted E coli pellets and incubation on ice with 5 ml ST buffer (20mM Tris/HCl, 200mM NaCl, pH 8.0) supplemented with lysozyme (1 mg/ml, L7651, Sigma-Aldrich), benzoase nuclease (5 unit/ml, Merck/Millipore, 71205-3) and 50 µl 100x Halt Protease Inhibitor Cocktail (Thermo Scientific 87785). After 2h of incubation, 100 µl of 10% (v/v) NP-40 (Thermo Fisher Scientific, 85124) was added to the lysate after which it was centrifuged (30 min, 40,000g, 4°C). The supernatant was added to 2 ml of Co^{2+} loaded HisPurTM Cobalt Superflow Agarose resin (Thermo Scientific, 25228) and incubated for at least 1 hour at 4 °C. The resin was washed with 9-10 times with 2 ml wash buffer (ST-buffer supplemented with 15 mM imidazole) until no detectable protein (as measured by OD 280) was washed from the resin. His-tagged proteins were eluted with 2x 1 ml elution buffer (ST buffer supplemented with 150 mM imidazole). The eluent was desalted and obtained in a 10 mM Tris-HCl pH 8.0 solution using Sephadex-G25 desalting columns (GE Healthcare 17-0852-

339 01). Proteins were short-term stored at 4 °C, or flash frozen and stored at -80 °C for long-term
340 storage.

341

342 *Spectroscopy*

343 *Extinction coefficient*

344 Purified proteins were diluted in PBS (50 mM Na_2HPO_4 – NaH_2PO_4, 137 mM NaCl, 2.7 mM KCl,
345 pH 7.4). Absorbance spectra were acquired with a spectrophotometer (Libra S70, Biochrom).
346 The spectra were recorded in the wavelength range of 260-700 nm, with a step size of 1 nm.
347 PBS was used as a background reference. The samples were diluted such that the absorbance
348 of the red chromophore peaked between 0.15 and 0.5. To denature the RFPs 10-200 µl 10 M
349 NaOH was subsequently added to the samples, which was directly mixed by pipetting. Spectra
350 were acquired continuously after addition of the sodium hydroxide until the absorbance
351 spectra showed a complete loss of the absorbance peak associated with the red chromophore
352 and displayed only the peak associated with the green chromophore at 457 nm. This
353 absorbance spectrum was used for further analysis, and if necessary, the average absorbance
354 value in the wavelength range 670 - 680 nm was subtracted from the spectra, in order to
355 correct for a minor offset. The concentration of the denatured green chromophore was
356 calculated assuming an extinction coefficient of 44,000 $M^{-1}cm^{-1}$ at 457 nm for the green
357 chromophore in the denatured RFP [16,17]. Based on the concentration of the red chromophore
358 the extinction coefficient for the red chromophore was determined at the maximum
359 absorbance wavelength. The above procedure was repeated at least three times per RFP
360 variant and the average extinction coefficient was calculated.

361

362 *Quantum yield*

363 Purified proteins were diluted in PBS (50 mM Na_2HPO_4 – NaH_2PO_4, 137 mM NaCl, 2.7 mM KCl,
364 pH 7.4). Absorbance spectra were recorded with a spectrophotometer (Libra S70, Biochrom)
365 in the wavelength range 260 - 700 nm with a step size of 1 nm. PBS was used as a background
366 reference. Three dilutions of each RFP variant were prepared with an absorbance at 540 nm
367 (A_{540}) of $0.005 < A_{540} < 0.05$. Fluorescence emission spectra were taken from the same sample

cuvette with a fluorimeter (Model FP-8500, Jasco with a red extended PMT tube model R928-23, operated by Jasco Spectral Manager v 2.15). The excitation wavelength was set at 540 nm, the emission spectrum was recorded from 550 to 800 nm with a step size of 1 nm at a scan speed of 200 nm·min^{-1}. The excitation as well as the emission slits were set at 2.5 nm. To obtain more accurate A_{540} absorbance values of the low absorbing samples, their absorbance spectra were fitted to an absorbance spectrum of the same RFP at high concentration (OD 0.1-0.3) and a variable (constant) offset value using a linear least squares fit. The A_{540} absorbance of the quantum yield samples was obtained from the fitted spectral component. Fluorescence spectra were background corrected by subtracting a spectrum measured with PBS. The emission spectra were corrected for spectral sensitivity using a calibrated white light source (ESC-842, Jasco) and the spectral area (I_{em}) was obtained by integrating from 550-800 nm. The absorbance at 540 nm (A_{540}) was plotted versus the area under the emission spectrum, subsequently the slope of the line was determined using linear regression. The regression lines were constrained to go through the origin, hence $I_{em} = a \cdot A_{540}$.

Equation 1 was used to calculate the quantum yield:

$$QY_s = QY_r \frac{a_s}{a_r} \qquad \textbf{Eq. 1}$$

In **Equation 1** *QY* denotes the quantum yield (*s* and *r* denote sample and reference RFP, respectively) and *a* corresponds to the acquired slope. mScarlet was used as a reference with a quantum yield of 0.704 [9].

Fluorescence lifetime

Fluorescence lifetime measurements of purified RFPs diluted in PBS (50 mM Na_2HPO_4 – NaH_2PO_4, 137 mM NaCl, 2.7 mM KCl, pH 7.4) were performed at an Olympus FV1000 confocal microscope equipped with a PicoHarp 300 TCSPC module (PicoQuant, Germany operated with SymPhoTime v 64.2.1) as described [9].

pH dependence of RFP fluorescence intensity

A pH buffer series was created (pH 3-10) using a universal 50 mM citric acid, 50 mM phosphoric acid and 50 mM boric acid, 100 mM NaCl buffer. Buffers at the desired pH were made by titrating a 2-times concentrated stock solution with 1M NaOH (Merck 109137) and adjusting the volume to obtain a two-fold dilution. Citric acid and phosphoric acid (85%) were from Merck (art 818707 and 563, respectively), boric acid was from Sigma (B-0252). The final pH value was measured 24h after preparation at room temperature and yielded pH values of 2.96, 3.90, 4.85, 5.94, 6.89, 8.16, 9.21 and 10.75. Fluorescence emission and absorbance Purified RFPs (section protein purification) were diluted in a black µ-clear 96 wells plate (655090, Greiner). For each pH triplicate samples for one RFP were made ranging from pH 3.0 to 10.8. With a Biotek FL-600 fluorescence plate reader using the KC4 v3.0 software, the fluorescence intensity was measured using a 555/25 excitation filter and a 620/40 emission filter. The curves of pH versus the fluorescence of the samples, *F*(pH)*,* was fitted using the Hill-function, **Equation 2** to obtain the apparent p*Ka* of the RFP and the Hill-coefficient *n*:

$$F(\mathrm{pH}) = \frac{F_{max}}{1+10^{n(\mathrm{p}Ka-\mathrm{pH})}} \qquad \textbf{Eq. 2}$$

For Fig. 1g data from 3 technical replicates were pooled into one data set for mScarlet3 and mScarlet-I3.

Stability at pH 13.5

Fluorescence intensity was monitored as a function of time in a fluorimeter (Model FP-8500, Jasco with a red extended PMT tube model R928-23) using 560 nm excitation and 610 nm emission (slits at 5 nm). Measurements were started with blank PBS solution (50 mM Na_2HPO_4 – NaH_2PO_4, 137 mM NaCl, 2.7 mM KCl, pH 7.4) to which 10 µl of purified RFP was added. After 1 min 100 µl of 2 M NaOH was added and the mixture was quickly mixed by pipetting up and down in the cuvette. To determine the stability of RFP fluorescence at alkaline pH, the blank intensity was subtracted and the signal was normalized to the blank-corrected RFP fluorescence signal at normal pH. The signal after addition of NaOH was corrected for dilution. After NaOH addition the final unbuffered NaOH concentration was 0.33 M, yielding a pH of 13.5. Stability measurements were perfomed in duplo yielding essentially similar results.

Cellular microscopy-based methods

Brightness mammalian cells

The brightness of the diverse RFPs was determined in U2Os and HeLa cells as described in [11]. Briefly, 50 ng of pDress vector encoding a 1:1 expression of mTurquoise2 cyan fluorescent protein and the respective RFP was mixed with 150 ng carrier DNA and transfected in mammalian cells in glass bottomed 24 well plates as described under general methods. 24 h after transfection cyan, yellow and red fluorescence images were recorded on a Nikon wide field microscope. The widefield microscope consisted of an Eclipse Ti-E (Nikon) equipped with 440, 508 and 555 nm LEDs (SpectraX, Lumencor). The excitation light from these LEDs was passed through a 440/20, 510/24 or 550/15 nm bandpasses, respectively. For 440 nm and 508 nm excitation, a triple-band cube (MXU74157, Nikon) was used, for 555 nm excitation a quad band cube (MXU 71640, Nikon) was used. Emission was additionally filtered with a 479/40, 550/49 nm or 593/46 nm bandpass (all from Semrock) placed in an optical filter changer (Lambda 10-B, Sutter instrument). For the three detected channels cyan, yellow and red, the effective excitation and emission bands were cyan: 430-450 nm excitation, 459-490 nm emission, yellow: 498-523 nm excitation, 526-555 nm emission, red: 543-558 nm excitation and 570-616 nm emission. A 10x CFI Plan Apochromat NA 0.45 (Nikon MRD00105) objective was used. Images were acquired on an ORCA-Flash4.0 V2 Digital CMOS camera (C11440-22CU, Hamamatsu Photonics) using Nikon NIS Elements AR v 4.51.01 64 bit. For each well a 5x5 tile of Images of 512 x 511 pixels each was acquired using a central ROI of 1024x1022 pixels with 2x2 binning and automated image stitching with 10% overlap, resulting in a final image size of 2253x2253 pixels corresponding to a 2.91x2.91 mm imaged area in each well. LED power was 10 %, 20% and 10% for 440, 508 and 555 nm LEDs for the cyan, yellow and red images, respectively. Integration time per image was 60 ms, 200 ms and 60 ms for the cyan, yellow and red images, respectively. The ratio of red to cyan fluorescence was calculated using the ratio_96-wells_macro_v7 as described [11]. The brightness in mammalian cells was obtained by correcting these ratios for spectral throughput of the imaging device. To this end, spectra of the corresponding purified RFPs were used and the average excitation in the 543-558 nm excitation bandpass was calculated from the normalized excitation spectrum and the integrated fluorescence in the 570-616 bandpass was divided by

458 the total integrated emission (550-800 nm). These corrections were normalized to the
459 throughput for mScarlet. Consequently, the detected Red/Cyan ratios were multiplied by 1.0
460 for mScarlet, 1.015 for mScarlet-I, 0.985 for mScarlet3, 0.964 for mScarlet-I3, 1.522 for
461 mCherry, 0.919 for mApple, 0.667 for TagRFP-T, 0.696 for mRuby3, 1.245 for FusionRed and
462 3.066 for mKate2 to obtain the relative cellular brightness values corrected for spectral
463 throughput. Cellular brightness experiments experiments were repeated at least 5 times in
464 different months and in different cell types and yielded essentially similar results.

465

466 *Brightness in mammalian cells after fixation.*

467 The brightness of the diverse RFPs following was also determined after paraformaldehyde
468 fixation in HeLa cells. Transfection, imaging and quantification was performed as described
469 above for living cells, but prior to determining the red to cyan fluorescence ratio, cells were
470 washed once with PBS and subsequently fixed for 20 minutes at room temperature with
471 freshly prepared 4% paraformaldehyde in PBS. After fixation, cells were washed once with
472 PBS and taken up in microscopy medium (140 mM NaCl, 5 mM KCl, 1 mM MgCl2, 1 mM CaCl2,
473 10 mM glucose, and 20 mM HEPES pH 7.4) and imaged on the same day.

474

475 *Maturation*

476 The extent of maturation was calculated by dividing the corrected cellular brightness by the
477 intrinsic brightness (see Extended Data Table I) for the respective RFP and normalizing to
478 mScarlet-I.

479 For measuring the maturation speed, the same cells, transfection and setup as described for
480 the brightness in mammalian cells was used. For image acquisition the yellow image was
481 omitted and cyan and red single image using the full sensor ROI at 2x2 binning was used.
482 Starting 5 hours after transfection, for each well in the 24 well plate a red and cyan image was
483 recorded every 15 minutes for 24 h. ROIs were manually drawn around 6-12 individual cells
484 in each timelapse that remained viable for prolonged time and showed steady FP
485 accumulation over time, but that started with no visible FP accumulation. The background
486 corrected average intensity in the ROI was calculated for both the cyan and red channels.

Subsequently, only traces that first showed a nonlinear increasing accumulation of both RFP and CFP fluorescence, followed by a linear increasing accumulation and ending with a slowing down of the increase were selected. Cells with discontinuous time traces (due to cell division or apoptosis) were discarded. The RFP and CFP trace were normalized to maximal intensity and a straight line was fitted to the curve at the point a maximal slope of normalized fluorescence increase with time was calculated. The intercept of this line with the time axis was calculated and the delay between the intercept found for the red and cyan curves were calculated for 6-15 individual cell traces and averaged.

FRET-FLIM

For all RFPs, direct fusion constructs with SYFP2 were generated using PCR- and restriction enzyme-based cloning. To enable a good comparison, the linker between the SYFP2 and RFP was chosen such that a constant number of amino acids separated the two beta barrels in the fusion construct (i.e. correcting for differences in the length of N- and C- termini). In Supplementary Table 1, the linker sequence between the different RFPs and SYFP2 is described for the constructs used for the FRET studies depicted in Fig. 1h and Extended Data Figs. 5.

50 ng of the SYFP2-RFP fusion constructs, SYFP2 or RFP single FP constructs, together with 150 ng of carrier DNA were transfected in HeLa cells growing in glass-bottomed 24-well plates as described above. 46 h after transfection, the samples were analyzed with FRET-FLIM with a frequency-domain widefield FLIM setup as described [11]. Briefly, the setup consisted of a Nikon TiE inverted fluorescence microscope, with a Proscan-III automated stage, excitation filter wheel and a Lambert Instruments FLIM Attachment (LIFA) system including a Multi-LED light source and a LI2CAM detector (Lambert Instruments) operated with LiFLIM v 1.2.23 . For measuring the SYFP2 lifetime a 506 nm LED modulated at 40 MHz was used (Lambert Instruments), and the excitation light was additionally filtered with a 500/24-nm excitation filter (BrightLine single-band bandpass filter; Semrock, cat. no. FF01-500/24). A filter cube with a 523-nm dichroic mirror (Semrock, cat. no. Di02-R514), and a 542/27-nm emission filter (BrightLine single-band bandpass filter; Semrock, cat. no. FF01-542/27-25) was used to separate excitation from the SYFP2 fluorescence emission. A 40× CFI Plan Apochromat NA

517 0.95 air objective (Nikon) was used. For determining the phase and modulation of the
518 modulated excitation light at the sample position, a diluted (OD < 0.05) Alexa488 (Thermo
519 Fisher Scientific) solution in PBS was used, for which a monoexponential fluorescence lifetime
520 of 4.03 ns was assumed. FLIM measurements were done in culture medium at 37 ˚C under 5-
521 7% CO_2 atmosphere. For each SYFP-RFP sample 3-4 FLIM stacks were acquired with a different
522 field of view of approximately 20 cells each. The mean lifetime of all cells in each FLIM stack
523 was determined and averaged for all stacks acquired from the same sample. Repeated
524 experiments with independent transfections yield essentially similar results.

525

526 *FRET-SPIM*

527 48h after transfection, the medium of the same samples as described under FRET-FLIM was
528 replaced with microscopy medium (140 mM NaCl, 5 mM KCl, 1 mM MgCl2, 1 mM CaCl2, 10
529 mM glucose, and 20 mM HEPES pH 7.4) and spectral images were acquired at room
530 temperature using a home-built spectral imaging setup as described [9,18]. Briefly the setup
531 consisted of a Zeiss Axiovert 200M fluorescence microscope, equipped with an HBO 100
532 Mercury lamp for excitation and an imaging spectrograph (Imspector V7, Specim, Finland)
533 coupled to a CCD camera (ORCA ER, Hamamatsu, Japan) operated using MatLab 6.1 with the
534 DCAMAPI interface. A 10x plan Neofluar NA 0.3 objective was used. Two spectral images were
535 recorded: one with a 500/20 nm excitation filter (Chroma Technology Incorporation), a 80/20
536 dichroic mirror (20/80bs, Chroma Technology Incorporation) and a LP530 nm emission filter
537 (#46-059, Edmund optics worldwide) to record the full spectra and one with a 577/20 nm
538 excitation filter, (D577/20, Chroma Technology Incorporation), a 596 nm dichroic mirror
539 (600dcxr, Chroma Technology Incorporation), and a 630/60 nm emission filter (HQ630/60,
540 Chroma Technology Incorporation) to record the direct excited RFP acceptor signal. The
541 spectra were extracted from the spectral images and analyzed as described [9]. Briefly, the
542 direct excited acceptor spectrum was subtracted from the FRET spectrum by analyzing the
543 spectra from single RFP transfected cells. Subsequently, the remaining donor and sensitized
544 emission acceptor signals were obtained by spectral unmixing with linear least squares
545 method using the unfused SYFP2 donor spectrum and unfused RFP acceptor spectrum as
546 reference. After spectral correction for detector sensitivity of the unmixed spectra, the
547 amount of donor quenching (δ_{loss}) was calculated from the net sensitized emission (α) and

548 the ratio of quantum yields of donor (Q_d) and acceptor (Q_a) according to $\delta_{loss} = \alpha\, Q_d/Q_a$.
549 The spectral components δ_{loss} and α are expressed as number of photons, obtained by
550 dividing the corrected unmixed sensitized emission spectrum by the unit area full emission
551 acceptor reference spectrum. From the donor quenching (δ_{loss}) and the remaining detected
552 donor (δ obtained by dividing the corrected unmixed remaining donor emission spectrum by
553 the unit area full emission donor reference spectrum) the energy transfer efficiency E is
554 calculated according to $E = \delta_{loss}/(\delta + \delta_{loss})$. Typically, 10-30 single cell spectra were
555 analyzed per SYFP2-RFP fusion. The averaged spectra were normalized to the unquenched
556 donor signal.

557

558 *Localization*

559 The Giantin DNA coding sequence of FRB–ECFP(W66A)–Giantin (67903, Addgene) was cloned
560 in to pmScarlet3–C1, using the restriction enzymes BsrGI and BamHI. The following constructs
561 pLifeAct–mTurquoise2 (36201, Addgene), pmTurquoise2–alphaTubulin (36202, Addgene),
562 pmTurquoise2–Peroxi (36203, Addgene), EB3-mTurquoise2 (98825, Addgene), LCK-
563 mTurquoise2 (98822, Addgene) and ER-mTurquoise2 (36204, Addgene) were digested with
564 AgeI and BsrGI to exchange mTurquoise2 for mScarlet3 yielding pLifeact-mScarlet3_N1
565 (189767, Addgene), pmScarlet3-alphaTubulin_C1 (189768, Addgene), pmScarlet3-Peroxi_C1
566 (189769), pEB3-mScarlet3_N1 (189770, Addgene), pLCK-mScarlet3_C1 (189771, Addgene)
567 and pER-mScarlet3_N1 (189772, Addgene), respectively. 4xmts-mScarlet3 and 3xnls-
568 mScarlet3 were created by digesting 4xmito-mNeongreen (Addgene 98875) and 3xnls-
569 mNeongreen (Addgene 98875) with AgeI and BsrGI to exchange mNeongreen for mScarlet3,
570 yielding p4xmts-mScarlet3_N1 (189774, Addgene) and p3xnls-mScarlet3_N1 (189775,
571 Addgene). LaminB-mTurquoise2 (99830, Addgene) was digested with AgeI and BglII to
572 exchange mTurquoise2 for mScarlet3 yielding pmScarlet3-LaminB_C1 (189776, Addgene).

573 HeLa cells (CCL-2, ATCC) were seeded in uncoated glass-bottomed 24 well plates (MatTek
574 P24G-1.5-13-F) and transfected with 50 ng plasmid, 150 ng carrier DNA and 2 µg PEI. 24h after
575 transfection, the cells were imaged in culture medium at 37 ˚C and 5% CO2 atmosphere using
576 a spinning disk setup as described [9]. Briefly this microscope system consisted of a Nikon
577 Eclipse Ti-E microscope equipped a 561 nm laser and a Yokogawa CSU X-1 spinning disk unit

(operating at 5,000 r.p.m.). The excitation light was directed to the sample via a custom-made dichroic mirror 405/488/561/640 through a 40× CFI Plan Apochromat NA 0.95 air objective (Nikon). The red fluorescence was filtered with a 585-675 nm bandpass (FF01-512/630-25 m, Semrock). Images were recorded with an iXon 897 EMCCD camera (Andor) controlled by Nikon NIS Elements AR v4.51.01 64-bit. Images shown are representative of 3-4 images taken from at least 2 technical replicates.

Photostability

For widefield photobleaching experiments transfection, mounting conditions and the microscope used were identical as described under brightness mammalian cells. A 20x Plan Fluor NA 0.5 air objective was used and the 555 nm LED was used set at 100% power. The quad band cube (MXU 71640, Nikon) and 593/46 nm bandpass emission filter was used for detection. Cells were focused under weak CFP illumination conditions in order to prevent any RFP bleaching prior to the actual photostability measurement. A time-lapse recording was made under perfect focusing at continuous 555 nm excitation with 25 steps of 5 s each. A 1024x1024 pixel central ROI of the camera was used at 1x1 binning and 10 ms integration time. The power at the object plane was 3.96 W/cm^2.

For confocal photobleaching, the transfection and mounting conditions were identical as described under brightness in mammalian cells. The microscope, the microscope objective and filter settings were identical as described under localization. The 561 nm laser was operated at 100% power, resulting in an illumination power at the object plane of 6.14 W/cm^2. Cells were focused under weak CFP illumination conditions in order to prevent any RFP bleaching prior to the confocal bleaching. Under perfect focusing at continuous 561 excitation 10 images separated by 100 ms were recorded, followed by 10 recordings separated by 400 ms, 10 recordings separated by 2 s, 10 recordings separated by 5s, 10 recordings separated by 10s and 10 recordings separated by 20 s, respectively, resulting in a final stack of 60 images each with an integration time of 50 ms.

Wide-field photostability was analyzed using the Bleach_96wells_macro_v9 macro as described [11]. On average 5-15 cells per image were used for this automated analysis. For analysis of the confocal photostability, the average fluorescence of 3-6 individual cells in each

608 recording was averaged and corrected for background fluorescence at each time point. The
609 intensities were normalized to the intensity at t_0. For both confocal and widefield
610 photostability measurements, the time axis was adjusted relative to (the uncorrected time
611 axis of) mScarlet to account for differences in excitation efficacy and RFP quantum yield to
612 mimic a situation where all RFPs start with emitting an equal number of photons/s per
613 molecule at t_0 as compared to mScarlet [12]. To estimate the time at which the FPs were
614 bleached by 50%, a linear interpolation method was used between the two most adjacent
615 time-points. Repeated experiments (3-4 times) yield essentially similar results.

616

617 *Prolonged confocal imaging*

618 For evaluating photostability under live cell confocal imaging conditions, pLifeact-
619 mScarlet3_N1 (189767, Addgene) was transfected in HeLa cells glass bottomed 24-well plates
620 that were imaged 24 h later using a commercial Leica SP8 confocal microscope with 561 nm
621 excitation (power at object plane 3 µW) using a 63x NA 1.4 HC PL APO CS2 oil immersion
622 objective operated with Leica LAS-X v 3.5.7.23325 64 bit. Fluorescence was recorded with a
623 HyD detector using a detection bandpass of 575-650 nm. 1000 frames were recorded with 2
624 scans averaged per frame over a period of 16 h with a frame rate of 1 frame/min at a (single
625 scan) pixel dwell time of 0.4 µs and pixel size of 0.18x0.18 µm.

626

627 *Photochromicity*

628 For photochromicity experiments, the transfection, mounting and microscope were identical
629 is described for the wide-field photostability measurements. RFPs were switched on with
630 100% 440 nm for 0.5 s (3.3 W/cm^2 at the focal plane) and subsequently illuminated at 20%
631 continuous 550 nm LED power (0.8 W/cm^2 at the focal plane) for 15 s during which images
632 were recorded every 300 ms. Five consecutive cycles of 440 nm on switching and 15 s of
633 continuous 550 illumination were executed were executed of which the 550 nm excited
634 recordings were concatenated in a stack of 255 images in total for each RFP. Data were
635 analyzed using the Bleach_96wells_macro_v9 macro [11] to extract the average time-traces.
636 Each trace represents the average of 6-13 cells per RFP variant. Photochromicity (P) was

637 calculated as described [9] from the RFP intensities just after 440 nm on-switching (I_a) and just
638 before 440 nm on-switching (I_b) as $P=(I_a-I_b)/I_a$. The 4 values found for the 5 consecutive
639 photochromicity cycles from the analysis of the average time traces per RFP were averaged
640 and indicated ± sd in Extended Data Table 1.

641

642 *Oligomerization analysis with OSER method*

643 mScarlet-CytERM-N17, mScarlet-I-CytERM-N17, TagRFP-T-CytERM-N17 and mCherry-
644 CytERM-N17 were cloned as described in [9]. FusionRed-CytERM-N17, mScarlet3-CytERM-N17
645 (189778, Addgene), mScarlet-I3-CytERM-N17 (189777, Addgene) and mScarlet-I3-NCwt-
646 CytERM-N17 (189779, Addgene) were cloned by digesting mCherry-CytERM-N17 with
647 enzymes AgeI and BsrGI to cut out mCherry and replace it with the other RFPs. Cells were
648 analyzed between 22h and 24 h after transfection. Imaging was performed with the same
649 microscope setup and transfection conditions as described under localization. To obtain an
650 overview of many cells, 16x16 tile scans were acquired with 10 % overlap and automated
651 image stitching in NIS elements software leading to 7040x7040 pixel images corresponding to
652 1.4x1.4 mm imaged areas in each well. Cells were analyzed as described in [13]. ROIs of
653 representative cells were assembled for Extended Data Fig. 4. Two days after transfection fast
654 moving punctate structures become visible in addition to the reticulate ER structure, likely
655 reflecting a degradation pathway involving the endolysosomal machinery. Using the same
656 spinning disk microscope, time-lapse imaging was performed at a frame interval of 0.32 s for
657 Supplementary Video 1. Repeated experiments (at least n=2) with independent transfections
658 yield essentially similar results.

659

660 *Cytotoxicity*

661 Cytotoxicity caused by expression of red fluorescent proteins in cells was tested with a
662 standard cell counting kit (96992, Sigma). This kit assesses living cells that produce NAD(P)H
663 to convert WST-8 (2-(2-methoxy- 4-nitrophenyl)-3-(4-nitrophenyl)-5-(2,4-disulfophenyl)-2H
664 tetrazolium, monosodium salt) into formazan that can be detected by its blue light
665 absorbance [19]. We used standard conditions for inducing expression of fluorescent proteins
666 by PEI mediated transient transfection of HeLa cells in 96 wells format [11,20]. On day 0, 3000

Hela cells were seeded per well in 100 µl DMEM in a Greiner (Cat. No. 655180) 96 well plate, which was subsequently placed in a 37 ˚C humidified incubator with 5% (v/v) CO_2. On day 1, 300 ng of mEGFP-pDx, pmScarlet-pDx, pmScarlet3-pDx (189754, Addgene), pmScarlet-I3-pDx (189756, Addgene), pmCherry-pDx or pmFusionRed-pDx was transfected with 1 µl 1 ‰ (w/v) PEI/ 19 µl optimum mix that was added per well in the 96 wells plate. As control, 300 ng empty pDx vector (carrier DNA) without an open reading frame was transfected. As blank we used wells without HeLa cells, that contained only 100 µl DMEM medium. After transfection, the 96 wells plate was returned to the humidified cell incubator. Under these conditions about 50-70% of the cells are transfected. On day 3, 48 h after transfection, 50 µl from a mix of 5.5 ml (containing 1 ml WST-8 cell counting kit, (96992, Sigma) and 4.5 ml DMEM), was added to each well followed by 2 h incubation at 37 ˚C and 5% CO_2. Then the absorbance at 460 nm was recorded using a Biotek FL-600 fluorescence/absorbance plate reader equipped with a 460/40 absorbance filter operated with BioTek KC4 v3.0. The average absorbance (± sd) of 6 wells that were transfected with the same plasmid was determined and corrected for blank to quantify possible cytotoxicity. The experiment shown in Fig. 1i was replicated 3 times and once in U2Os cells with similar results.

Cell viability

On day 0, 2.5 µg of mEGFP-pDx, pmScarlet-pDx, pmScarlet3-pDx (189754, Addgene), pmScarlet-I3-pDx (189756, Addgene), pmCherry-pDx or pmFusionRed-pDx was transfected into HeLa cells cultured in T25 flasks. After approximately 4h, the medium was refreshed. Cells were cultured as described under general methods. Cells were passaged at day 2. At day 2 trypsinized control mEGFP cells were mixed with each of the RFP transfected cells. From the 5 resulting cell mixtures, 4-5 biological replicates were subsequently grown in T25 flasks and passaged on day 4 and on day 6. During passaging on day 2, 4 and 6, two aliquots of (mixed) trypsinized cells were transferred to glass-bottomed 24-well plates supplemented with 0.5 ml culture medium. After 4-5 h of incubation at at 37 °C under 7% humidified CO2 atmosphere, the 24-well plates were analyzed for the number of cells displaying green and red fluorescence by fluorescence microscopy, amounting to 8-10 red/green cell number ratios per time point per RFP. For microscopy, the same setup was used as described for the brightness in mammalian cells. For GFP detection a 470 nm LED and for RFP detection a 555

nm LED (SpectraX, Lumencor) was used. The excitation light from these LEDs was passed through 470/24 or 550/15 nm bandpasses, respectively. A quad band cube (MXU 71640, Nikon) was used. Emission was additionally filtered with a 527/70 or 593/46 nm bandpass (both from Semrock) placed in an optical filter changer (Lambda 10-B, Sutter instrument). For the green and red detected channels, the effective excitation and emission bands were green: 458-483 nm excitation, 492-541nm emission, and red: 543-558 nm excitation and 570-616 nm emission. A 10x CFI Plan Apochromat NA 0.45 (Nikon MRD00105) objective was used. Images were acquired on an ORCA-Flash4.0 V2 Digital CMOS camera (C11440-22CU, Hamamatsu Photonics). For each well a 12x12 tile of Images of 512 x 511 pixels each were acquired using a central ROI of 1024x1022 pixels with 2x2 binning and automated image stitching with 10% overlap, resulting in a final image size of 2 channels of 5300x5300 pixels corresponding to a 6.84x6.84 mm imaged area in each well. LED power was 50 % and 20% for 470 nm and 555 nm LEDs for the green and red images, respectively. Integration time per image was 100 ms, for each exposure. Between 100 and 3000 fluorescent cells were counted per well for each color using an automated ImageJ macro. Briefly this macro first reduced noise, performed a background correction and applied a threshold intensity after which individual cells were automatically counted using the analyze particles ImageJ command. The threshold intensity for the green channel was identical for all analyzed samples, the threshold intensity for the red channel was different for each RFP to account for differences in cellular brightness, but identical for samples from different days. The effective cellular brightness of the different RFPs was determined as described under brightness mammalian cells by analyzing HeLa cells 48 h after transfection with pDress constructs driving expression of mTurquoise2 and the respective RFPs in a 1:1 ratio. The relative brightness and RFP thresholds were 1.307 for mScarlet, 1.899 for mScarlet3, 1.872 for mScarlet-I3, 0.331 for mCherry and 0.298 for FusionRed. This resulted in final thresholds of 24 counts for cells expressing GFP and 100 times the above relative brightness values for the RFP channel thresholds. For each sample (RFP mixture, time point and replicate) the ratio of red fluorescent cells over green fluorescent cells was calculated, normalized to the ratio obtained at day 2 (to correct for possible differing transfection efficiencies) and displayed.

Structure determination

A batch of mScarlet3 protein sample was specifically expressed and purified for crystallization purposes.

Protein expression.

Bacterial transformation of the pDX vector was achieved in E. coli BL21(DE3) (Invitrogen) and incubated overnight at 30 ºC on Kanamycin (30 µg/mL) selective LB-agar plates. A starting culture of 100 mL of LB supplemented with Kanamycin (30 µg/mL) was grown overnight at 37 ºC under agitation (165 rpm). 1 L of LB supplemented with Kanamycin (30 µg/mL) was inoculated with 10 mL of starting culture, then grew at 37 ºC, 145 rpm until the D.O. (600 nm) reached 0.6. Protein expression was then induced with L-rhamnose at a final concentration of 0.2 %, and grew overnight at 20 ºC, 145 rpm.

Purification.

Cultures were centrifugated at 4000 g for 30 min at 4 °C. The pellets were then resuspended in 25 mL of lysis buffer (50 mM Tris pH 8.0, 300 mM NaCl, 10 mM imidazole, 20 mM $MgSO_4$, 1 tablet of the EDTA-free protease inhibitor cocktail complete (Roche, Basel, Switzerland), 400 µg/mL DNAse) per liter of culture, flash-frozen and stored at -80 ºC overnight. Thawed pellets were sonicated and cell debris were centrifuged at 18,000 g for 45 min at 4 ºC. The clarified lysate was then loaded on nickel affinity Histrap HP 1 mL (Cytiva) column for protein purification. Proteins were eluted against an imidazole buffer (20 mM Tris pH 8.0, 200 mM NaCl, 500 mM imidazole) with isocratic elution (5 to 500 mM imidazole in 10 % increments). The final purification step consisted in a size exclusion chromatography using a HiPrep 16/60 Sephacryl 100 S HR column (Cytiva) against a 20 mM Tris pH 8.0 buffer. Purified mScarlet-3 proteins were concentrated to 15 mg/mL using an Amicon 15 (10 kDa cutoff, Merck Millipore) for further crystallization assays.

Protein crystallization and crystal harvesting.

Crystallization conditions were set up in 96-well CrystalDirect plates using commercial screens available at the HTX lab crystallization platform (https://htxlab.embl.fr/, EMBL Grenoble). These plates are suitable for automated crystal harvesting based on photoablation of the cover film [21]. A condition consisting of 0.1 M NaCl, 0.1 M HEPES pH 7.5 and 1.6 M ammonium sulphate in a mother liquor/protein ratio of 1:2 yielded a crystal of 800 x 400 x 200 μm^3. The position of the crystal was marked using the Crystal Harvesting Interface provided within the plate viewing function of the CRIMS (Crystallographic Information Management System) system and used for automated harvesting and flash-cooling of the sample. Cryoprotection was achieved by removing excess of mother liquor around the crystal by aspiration prior to crystal harvesting without addition of any cryoprotectant molecule.

Data collection, processing and structure refinement.

The data collection was performed at 100 K at beamline ID30B of the ESRF [22] using an X-ray detector Pilatus3 6M (Dectris). Data were integrated using the automated processing pipeline [22] accessible in the extended Laboratory Information Management System ISPyB (https://exi.esrf.fr/) [23]. The best data integration was obtained with the XDSAPP pipeline and yielded structure factors in the $P2_12_12_1$ space group he at 1.33 Å resolution using a $CC_{1/2}$ resolution cut-off of 0.5. Data collection statistics can be found in Supplementary Table 2. The structure was solved by the molecular replacement method with PHASER v2.8.3 [24] using the previously-determined structure mScarlet structure (PDB ID: 5LK4) [9]. The asymmetric unit is composed of two molecules of mScarlet3. Cycles of structure refinement and model rebuilding upon electron density map inspection were performed using REFMAC v5.8.0267 [25] and COOT [26], respectively. In the Ramachandran plot, 98.3% of residues are in the favoured region, 1.7% are in the allowed region and 0.0% are outliers. Only 0.5% of side chain rotamers are outliers. Structure refinement statistics can be found in Supplementary Table 2. The structure of mScarlet3 at pH 7.5 has been deposited in the Protein Data Bank under PDB ID: 7ZCT.

Zebrafish larvae experiments

Wild-type zebrafish (AB) larvae were maintained at 28 °C in E3 medium. Injections were performed on fertilized zebrafish eggs at the one cell stage.

Episomal expression was assessed by injecting pDRESS_mTurquoise2_spatial-linker-P2A_mScarlet3 (189752, Addgene) and pDRESS_mTurquoise2_spatial-linker-P2A_mScarlet3 (130509, Addgene) [11] at a concentration of 250 ng/µl. After 24 hours, the larvae were fixed in 4% paraformaldehyde and subsequently analyzed on a confocal microscope with a 40x PLAN Apochromat 1.3 NA objective (SP8X, Leica Microsystems). A white light laser set at 405 nm (7.5%) and 569 nm (25%) was used to excite mTurqouise2 (Em:450-525) and mScarlet or mScarlet3 (Em 580-655nm), respectively. For quantification, the relative fluorescence intensity of the mScarlet(3) channel compared with the mTurquoise2 channel was calculated for 35 regions of interest per construct.

Expression of mScarlet3 in the pancreas was allowed by placing mScarlet3 under the control of the ElastaseA promoter in a Tol2 backbone and co-injecting this with Tol2 transposase mRNA, both at 250ng/µl [27–29]. The Tol2 plasmid was a kind gift of Dr. Kawakami, Japan [28,30]. After te24 hours, pigment formation was inhibited by adding 1-phenyl 2-thiourea (PTU) to a final concentration of 0.2 mM. Time-lapse imaging was performed on a single-plane illumination microscope with a 10x PLAN Apochromat 0.5 NA detection objective (LS7, Zeiss) at 15-min intervals for 12 hours with a Z-stack of 79 frames taken at each timepoint with 1.73 µm intervals using Zeiss Zen Black v3.1. Here, the zebrafish larva was illuminated through the ventral and dorsal sides with a 561 laser and detection was done through a 575-615 nm band pass filter with a camera set at 120 ms exposure time. For the illustration (Fig. 2j, Supplementary Video 5), only the images originating from ventral sided illumination were used. A maximum intensity projection of 21 frames in Z, surrounding a dividing cell, was generated and time alignment with linear interpolation and subsequent cropping was performed to account for drift over time (Zen blue v3.0, Zeiss). The image represents a single experiment.

For the analysis of H2B-mScarlet3 in zebrafish larvae, mScarlet3 cDNA was cloned in frame with histone 2B and subsequently cloned in the pCS2+ backbone containing the SP6 promotor. Capped RNA was *in vitro* transcribed using the mMESSAGE mMACHINE SP6 Transcription Kit (Invitrogen, AM1340) and subsequently cleaned up using MEGAclear Transcription Clean-Up Kit (Invitrogen, AM1908). Zebrafish embryos were micro-injected with the capped RNA in the 1-cell stage and incubated in E3 medium containing 0.2 mM N-

phenylthiourea (PTU) (Sigma Aldrich, P7629) to inhibit pigment formation. At 30 hours post-fertilization (hpf) the zebrafish embryos were sedated using 0.2 g/L ethyl 3-aminobenzoate (Tricaine, MS-222) (Sigma Aaldrich, E10521). For Fig. 2k and Supplementary Videos 6 and 7 imaging was performed on a single-plane illumination microscope using a 10X Plan Apochromat 0.5 NA detection objective (LS7, Zeiss). Z-stack images were recorded with 1 µm intervals over 309 frames with 5 min intervals for 6 hours. Here, the zebrafish embryo was excited from the ventral and dorsal sides with a 561nm laser and detection of the saggital plane was done using a 585nm long pass filter with the camera set at 100ms exposure time (this is a first experiment that was immediately successful).

Reporting Summary

Further information on research design is available in the Nature Research Reporting Summary linked to this article.

Data availability

The data supporting this study are available within the article and the Supplementary Information including the digital data underlying the figures. Other (raw) data supporting this study will be available from the corresponding author upon reasonable request. Plasmids constructed in this study, their maps, and sequences were deposited to the non-profit organization Addgene ID: 189752-189779. The mScarlet3 crystal structure was deposited at the Protein Data Bank as PDB ID: 7ZCT.

Code availability

Image analysis was performed in ImageJ/Fiji using macros described in [11] and the code is available on GitHub (see https://github.com/molcyto/MC-FLIM-Petri-dish, https://github.com/molcyto/MC-Ratio-Petri-dish, https://github.com/molcyto/MC-FLIM-96-wells, https://github.com/molcyto/MC-Ratio-96-wells, https://github.com/molcyto/MC-Bleach-96-wells).

Methods-only references

16. Gross, L. A., Baird, G. S., Hoffman, R. C., Baldridge, K. K. & Tsien, R. Y. The structure of the chromophore within DsRed, a red fluorescent protein from coral. *Proc Natl Acad Sci U S A* **97**, 11990–11995 (2000).
17. Shagin, D. A. *et al.* GFP-like Proteins as Ubiquitous Metazoan Superfamily: Evolution of Functional Features and Structural Complexity. *Mol Biol Evol* **21**, 841–850 (2004).
18. Vermeer, J. E. M., van Munster, E. B., Vischer, N. O. & Gadella Jr., T. W. J. Probing plasma membrane microdomains in cowpea protoplasts using lipidated GFP-fusion proteins and multimode FRET microscopy. *J Microsc* **214**, 190–200 (2004).
19. Aslantürk, Ö. S. In Vitro Cytotoxicity and Cell Viability Assays: Principles, Advantages, and Disadvantages. in *Genotoxicity - A Predictable Risk to Our Actual World* (InTech, 2018). doi:10.5772/intechopen.71923.
20. Dabbaghi, M., Hashemi, K., Oskuee, R. K. & Afkhami-Goli, A. Reverse relation between cytotoxicity and Polyethylenimine/DNA ratio, the effect of using HEPES-buffered saline (HBS) medium in gene delivery. *Toxicology in Vitro* **83**, (2022).
21. Cipriani, F. *et al.* CrystalDirect: A new method for automated crystal harvesting based on laser-induced photoablation of thin films. *Acta Crystallogr D Biol Crystallogr* **68**, 1393–1399 (2012).
22. McCarthy, A. A. *et al.* ID30B – a versatile beamline for macromolecular crystallography experiments at the ESRF. *J Synchrotron Radiat* **25**, 1249–1260 (2018).
23. Delagenière, S. *et al.* ISPyB: An information management system for synchrotron macromolecular crystallography. *Bioinformatics* **27**, 3186–3192 (2011).
24. McCoy, A. J. *et al.* Phaser crystallographic software. *J Appl Crystallogr* **40**, 658–674 (2007).
25. Murshudov, G. N. *et al.* REFMAC5 for the refinement of macromolecular crystal structures. *Acta Crystallogr D Biol Crystallogr* **67**, 355–367 (2011).
26. Emsley, P., Lohkamp, B., Scott, W. G. & Cowtan, K. Features and development of Coot. *Acta Crystallogr D Biol Crystallogr* **66**, 486–501 (2010).
27. Kawakami, K. Tol2: A versatile gene transfer vector in vertebrates. *Genome Biol* **8**, 1–10 (2007).
28. Kawakami, K. *et al.* A transposon-mediated gene trap approach identifies developmentally regulated genes in zebrafish. *Dev Cell* **7**, 133–144 (2004).

879 29. Wan, H. *et al.* Analyses of pancreas development by generation of gfp transgenic
880 zebrafish using an exocrine pancreas-specific elastaseA gene promoter. *Exp Cell Res*
881 **312**, 1526–1539 (2006).
882 30. Urasaki, A., Morvan, G. & Kawakami, K. Functional dissection of the Tol2 transposable
883 element identified the minimal cis-sequence and a highly repetitive sequence in the
884 subterminal region essential for transposition. *Genetics* **174**, 639–649 (2006).
885
886

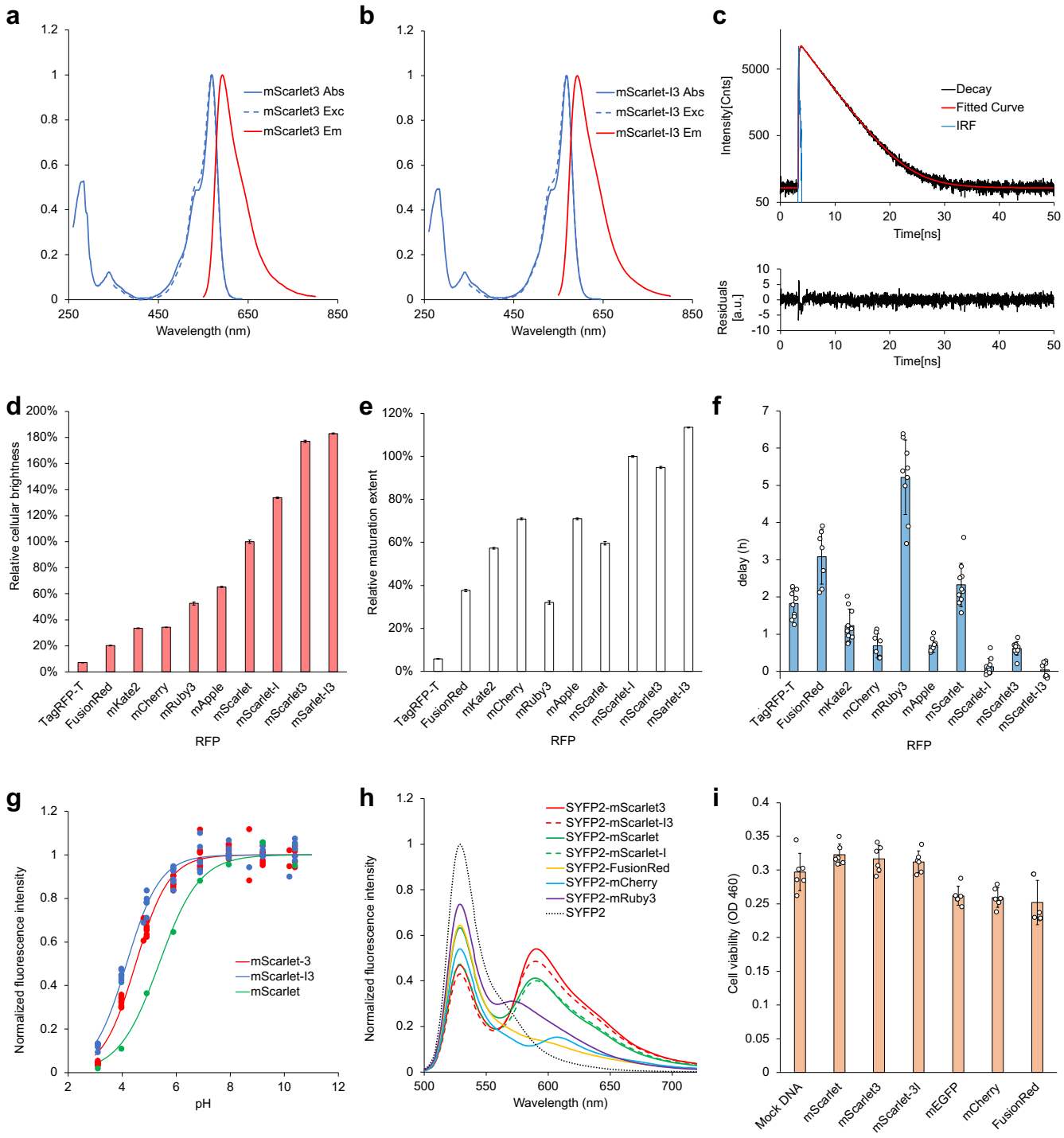
a
mScarlet3 Abs
mScarlet3 Exc
mScarlet3 Em
Wavelength (nm)
b
mScarlet-I3 Abs
mScarlet-I3 Exc
mScarlet-I3 Em
Wavelength (nm)
c
Decay
Fitted Curve
IRF
Intensity[Cnts]
Time[ns]
Residuals [a.u.]
Time[ns]
d
Relative cellular brightness
TagRFP-T
FusionRed
mKate2
mCherry
mRuby3
mApple
mScarlet
mScarlet-I
mScarlet3
mScarlet-I3
RFP
e
Relative maturation extent
RFP
f
delay (h)
RFP
g
Normalized fluorescence intensity
mScarlet-3
mScarlet-I3
mScarlet
pH
h
SYFP2-mScarlet3
SYFP2-mScarlet-I3
SYFP2-mScarlet
SYFP2-mScarlet-I
SYFP2-FusionRed
SYFP2-mCherry
SYFP2-mRuby3
SYFP2
Normalized fluorescence intensity
Wavelength (nm)
i
Cell viability (OD 460)
Mock DNA
mScarlet
mScarlet3
mScarlet-3I
mEGFP
mCherry
FusionRed

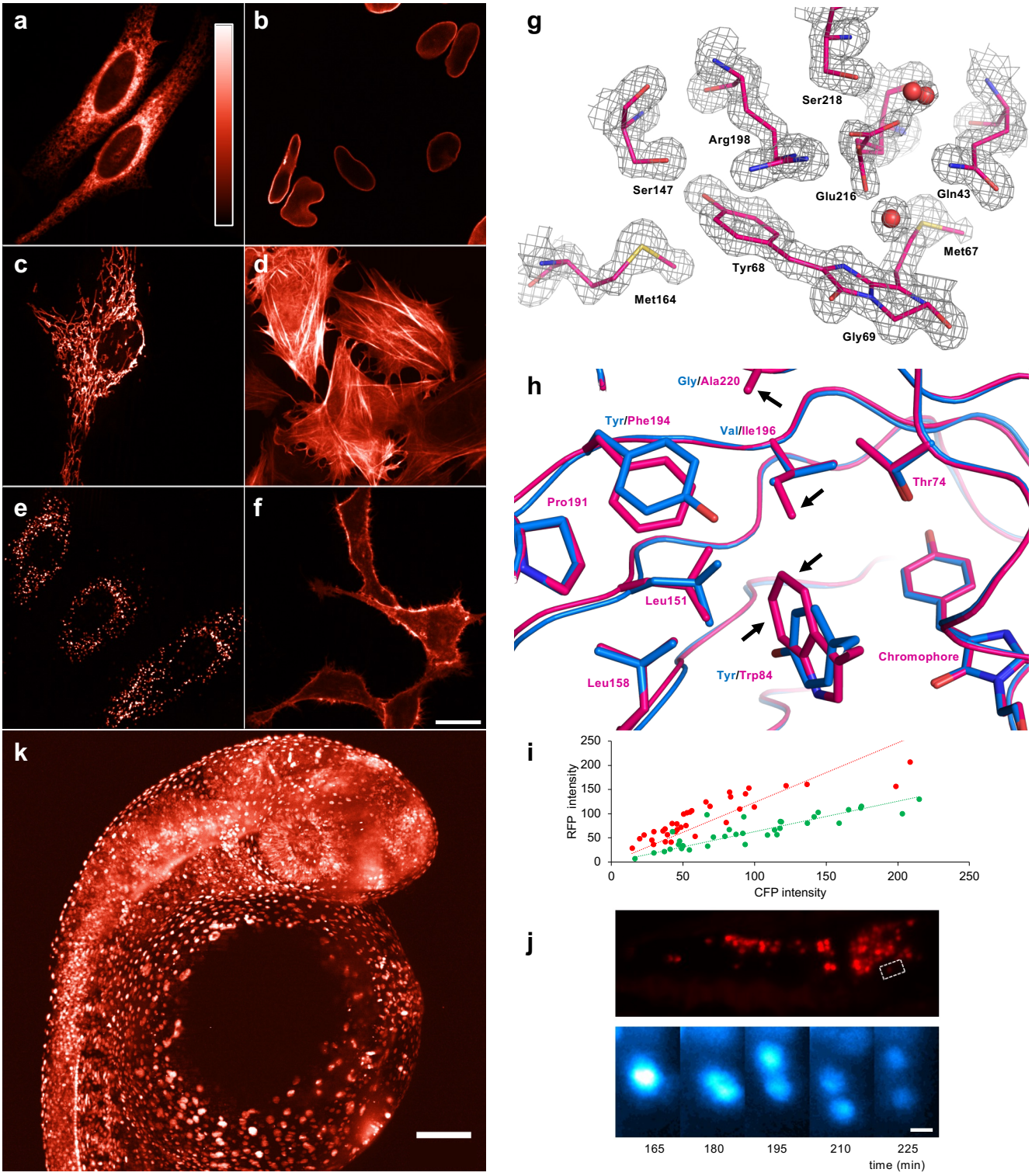
a
b
c
d
e
f
k
g
Ser218
Arg198
Ser147
Glu216
Gln43
Met67
Tyr68
Met164
Gly69
h
Gly/Ala220
Tyr/Phe194
Val/Ile196
Thr74
Pro191
Leu151
Chromophore
Leu158
Tyr/Trp84
i
RFP intensity
CFP intensity
0
50
100
150
200
250
j
165
180
195
210
225
time (min)

	Spectroscopic Characteristics												Brightness		Photostability			Maturation		Stability pH13.5		Ratio FRET	Monomeric Assay		
	Abs max[a] (nm)	Em max[b] (nm)	ε[c] 10^3 $M^{-1}cm^{-1}$	QY[d] (%)	τ_1[e] (ns)	τ_2[f] (ns)	α_1[g] (%)	χ^2[h]	τ_{avg}[i] (ns)	τ_M(cells)[j] (ns)	pK_a[k]	n[l]	EC*QY[m]	Cells[n] % 24h	WF $t_{1/2}$[o] (s)	Confocal $t_{1/2}$[p] (s)	PC[q] %	Accum[r] (% mSc-I)	delay[s] (h)	I_0[t] (%)	$t_{1/2}$[u] (min)	Sens em[v] (%)	Correct ER[w] (%)	# OSER[x] (%)	cells[y] n
mScarlet3	569	592	104±1	75.1±1	3.96±0.01	x	100	1.15	3.96	3.67±0.00	4.5±0.1	0.70+0.04	78±1	177±1	52	27	<1%	94.9±0.5	0.6±0.2	86	45.6	140±7	85	7	139
mScarlet-I3	568	592	105±2	64.5±1.1	3.64±0.01	x	100	1	3.64	3.35±0.00	4.2±0.1	0.70±0.04	69±2	183±1	47	16	1.1±0.3%	113.5±0.3	0.0±0.2	63	2.24	129±5	87	5	204
mScarlet-I3-NCwt	568	592	102±0.5	65.3±0.8	3.63±0.01	x	100	1.25	3.63	3.33±0.03	4.2±0.1	0.76±0.16	68±1	177±1	46	15		115±1	-	70	2	136±9	87	0	61
mScarlet	569	593	*100±3*	*70.4±0.8*	*3.86±0.01*	*x*	*100*	*1.12*	*3.86*	3.53±0.01	*5.3±0.2*	*0.79±0.22*	*71±2*	100±1	62	29	<1%	60±1	2.3±0.6	<0.5	x	92±23	92	8	39
mScarlet-I	569	594	*104±3*	*54±4*	*3.52±0.02*	*1.67±0.04*	*76±1*	*1.11*	*3.08*	3.01±0.04	*5.4±0.4*	*0.52±0.19*	*57±4*	134±1	55	21	<1%	100.0±0.4	0.1±0.2	<0.5	x	100±6	84	8	80
mRuby3	557	591	127±0.3	54±1	2.80±0.01	x	100	1.04	2.80	2.49±0.02	*4.8*		69±1	53±1	*	*	42±1%	32±1	5.2±1.0	50	0.53	50±24	0	24	17
mKate2	588	631	*63±3*	*39±1*	*2.47±0.01*	*x*	*100*	*1.21*	*2.47*	2.53±0.01	*5.4*		*25±1*	33.5±0.3	96	32	<1%	57.3±0.3	1.2±0.4	62	0.58		56	12	68
Tag-RFP-T	556	585	*110±7*	*48±1*	*2.66±0.02*	*1.44±0.06*	*72±3*	*1.12*	*2.32*	2.44±0.02	*4.6*		*53±2*	7.1±0.1	*	*	27±3%	5.6±0.1	1.8±0.4	<0.5	x		31	66	182
mCherry	586	610	*88±1*	*23±1*	*1.28±0.03*	*2.00±0.07*	*71±0*	*1.08*	*1.49*	1.56±0.01	*<4.5*		*20±1*	34.2±0.2	55	32	<1%	70.9±0.4	0.7±0.3	<0.5	x	37±3	82	18	87
FusionRed	575 *580ex*[z]	605 *608*[z]	93 *94.5*[z]	24±1 *19*[z]	1.58±0.03	2.72±0.15	84±4	1.01	1.76	1.71±0.03	*4.6*[z]		22 *18*[z]	20.3±0.3	*	*	26±0.2%	37.6±0.6	3.1±0.7	40	0.48	31±5	67	4	99
dTomato	555	583	*90±1*	*69±1.3*	*3.47±0.01*	*1.21±0.07*	*95±0*	*1.36*	*3.36*	3.28±0.02	*4.7*		*62±1*	116±1	154	14	<1%	112±2	1.6±0.4	<0.5	x		17	82	266

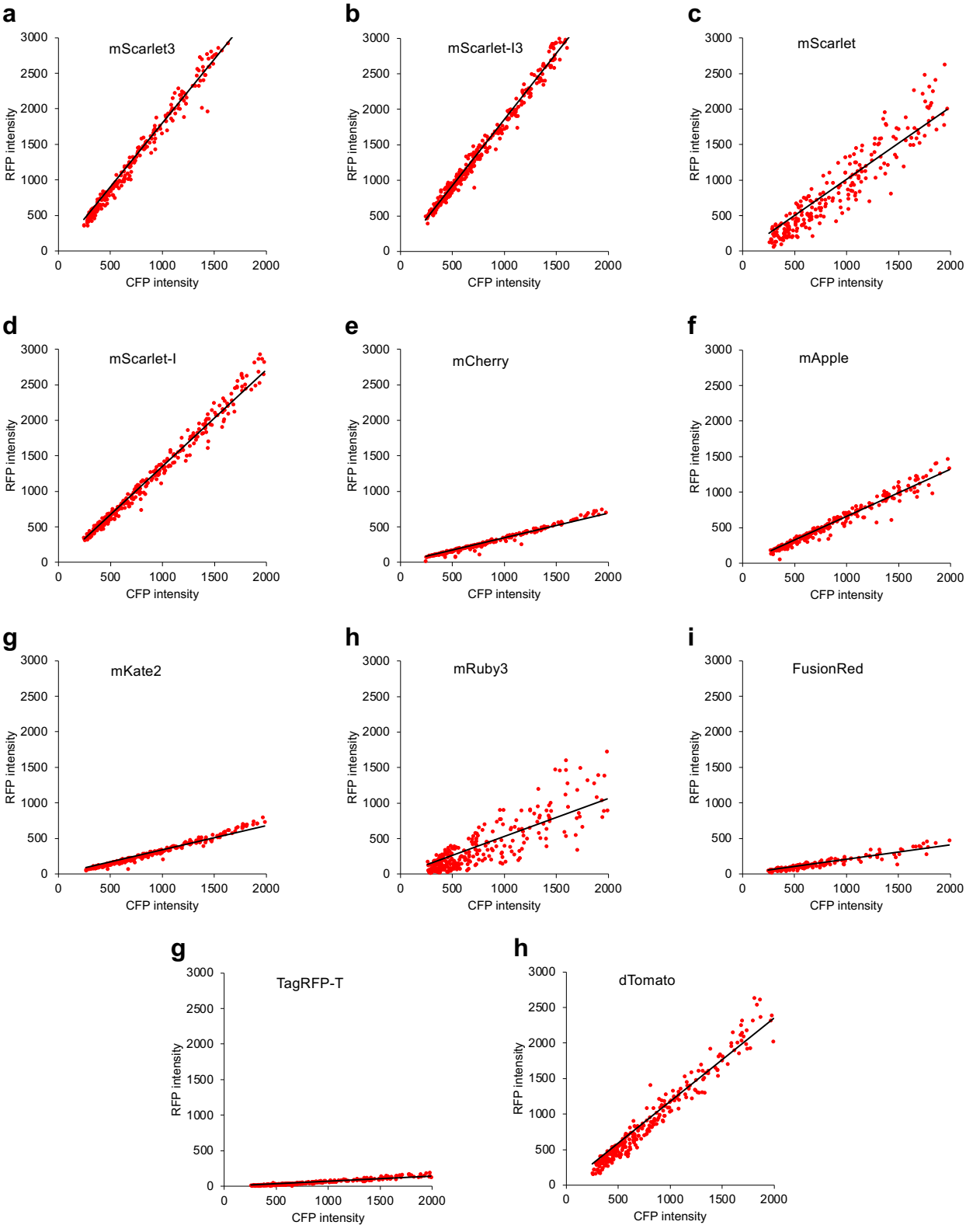
a
mScarlet3
b
mScarlet-I3
c
mScarlet
d
mScarlet-I
e
mCherry
f
mApple
g
mKate2
h
mRuby3
i
FusionRed
g
TagRFP-T
h
dTomato
RFP intensity
CFP intensity
0
500
1000
1500
2000
2500
3000

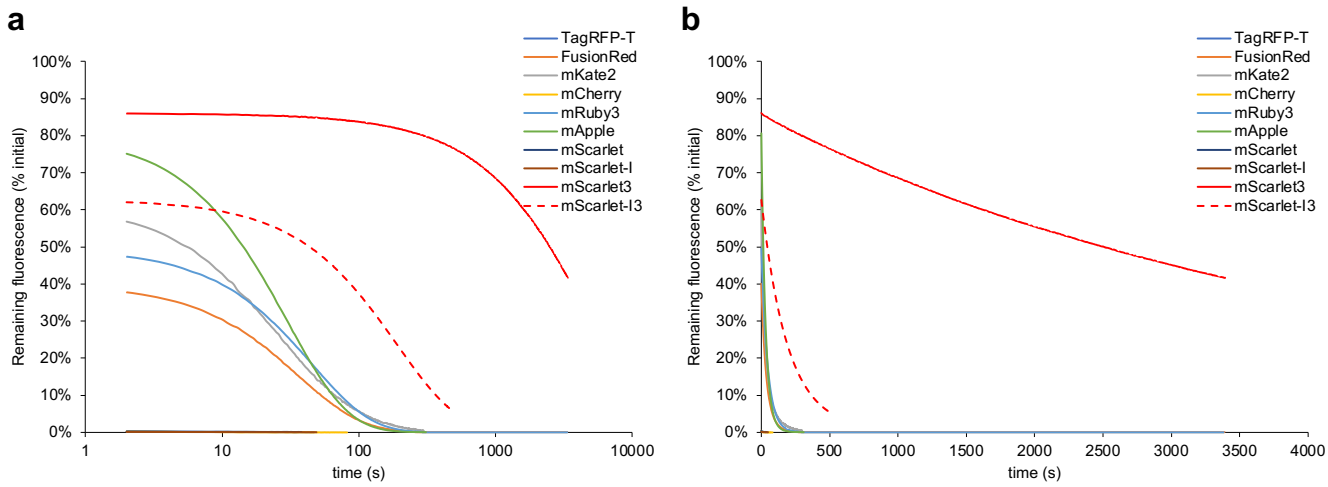
a
b
TagRFP-T
FusionRed
mKate2
mCherry
mRuby3
mApple
mScarlet
mScarlet-I
mScarlet3
mScarlet-I3
Remaining fluorescence (% initial)
time (s)
100%
90%
80%
70%
60%
50%
40%
30%
20%
10%
0%
1
10
100
1000
10000
0
500
1000
1500
2000
2500
3000
3500
4000

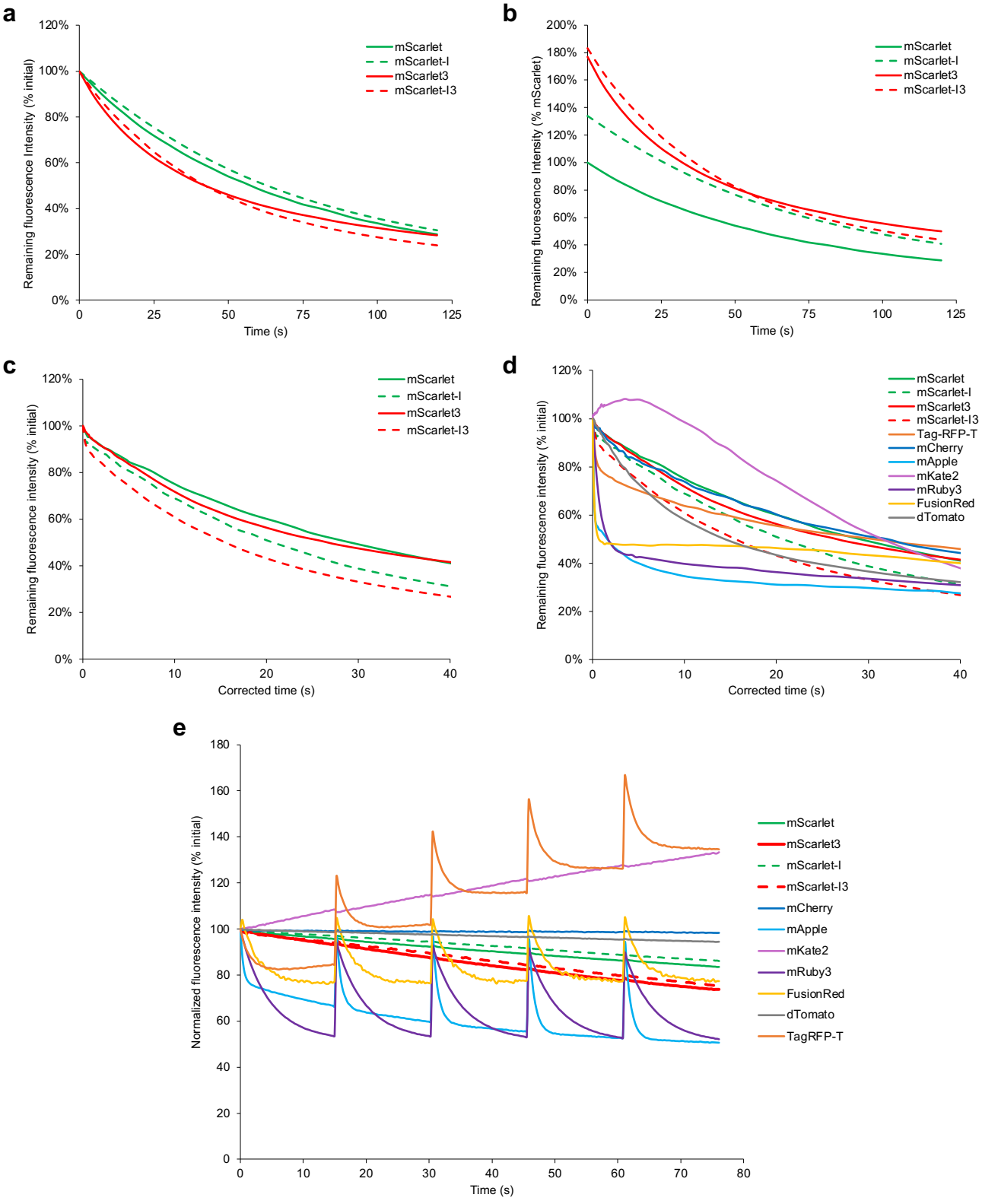
a
Remaining fluorescence Intensity (% initial)
120%
100%
80%
60%
40%
20%
0%
0
25
50
75
100
125
Time (s)
mScarlet
mScarlet-I
mScarlet3
mScarlet-I3
b
Remaining fluorescence Intensity (% mScarlet)
200%
180%
160%
140%
120%
100%
80%
60%
40%
20%
0%
0
25
50
75
100
125
Time (s)
mScarlet
mScarlet-I
mScarlet3
mScarlet-I3
c
Remaining fluorescence intensity (% initial)
120%
100%
80%
60%
40%
20%
0%
0
10
20
30
40
Corrected time (s)
mScarlet
mScarlet-I
mScarlet3
mScarlet-I3
d
Remaining fluorescence intensity (% initial)
120%
100%
80%
60%
40%
20%
0%
0
10
20
30
40
Corrected time (s)
mScarlet
mScarlet-I
mScarlet3
mScarlet-I3
Tag-RFP-T
mCherry
mApple
mKate2
mRuby3
FusionRed
dTomato
e
Normalized fluorescence intensity (% initial)
180
160
140
120
100
80
60
40
20
0
0
10
20
30
40
50
60
70
80
Time (s)
mScarlet
mScarlet3
mScarlet-I
mScarlet-I3
mCherry
mApple
mKate2
mRuby3
FusionRed
dTomato
TagRFP-T

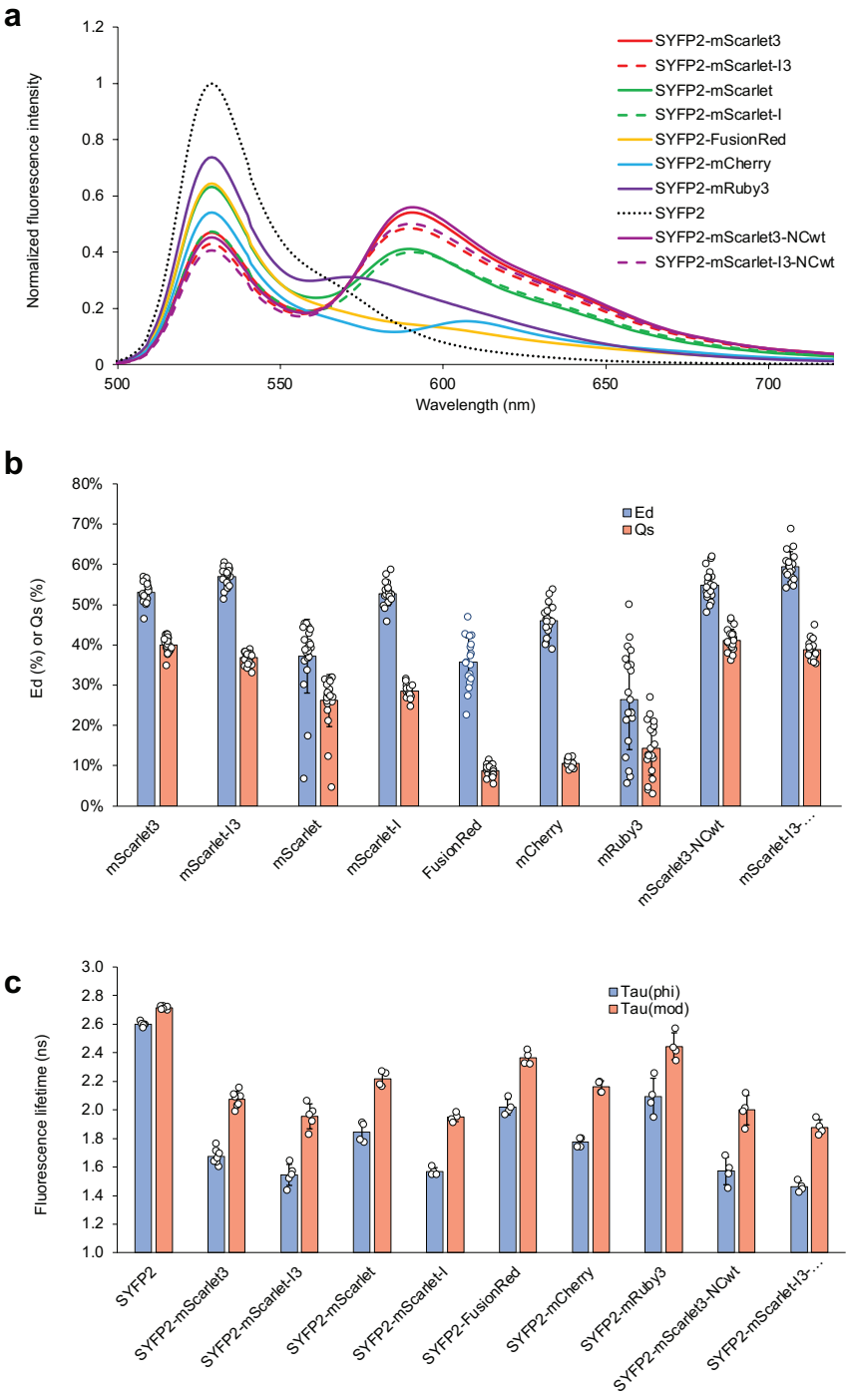
a
Normalized fluorescence intensity
Wavelength (nm)
SYFP2-mScarlet3
SYFP2-mScarlet-I3
SYFP2-mScarlet
SYFP2-mScarlet-I
SYFP2-FusionRed
SYFP2-mCherry
SYFP2-mRuby3
SYFP2
SYFP2-mScarlet3-NCwt
SYFP2-mScarlet-I3-NCwt
b
Ed (%) or Qs (%)
Ed
Qs
mScarlet3
mScarlet-I3
mScarlet
mScarlet-I
FusionRed
mCherry
mRuby3
mScarlet3-NCwt
mScarlet-I3-…
c
Fluorescence lifetime (ns)
Tau(phi)
Tau(mod)
SYFP2
SYFP2-mScarlet3
SYFP2-mScarlet-I3
SYFP2-mScarlet
SYFP2-mScarlet-I
SYFP2-FusionRed
SYFP2-mCherry
SYFP2-mRuby3
SYFP2-mScarlet3-NCwt
SYFP2-mScarlet-I3-…

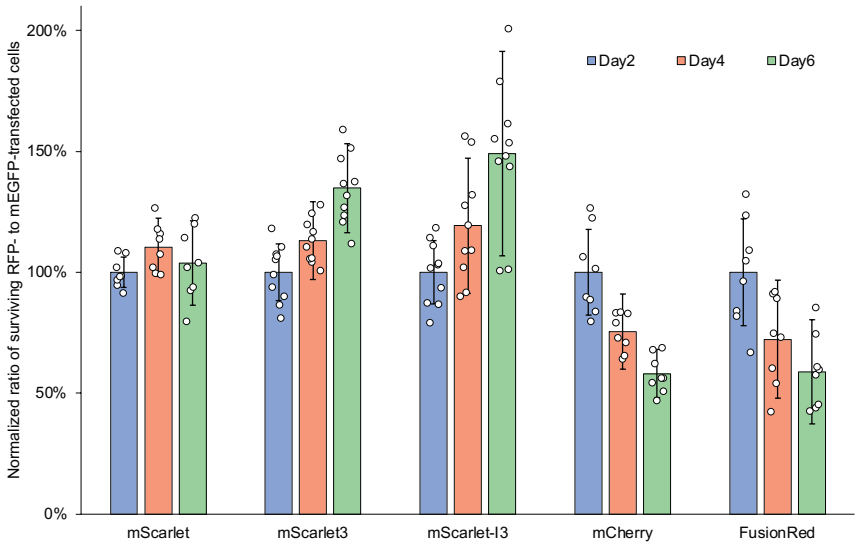
Normalized ratio of surviving RFP- to mEGFP-transfected cells
200%
150%
100%
50%
0%
Day2
Day4
Day6
mScarlet
mScarlet3
mScarlet-I3
mCherry
FusionRed

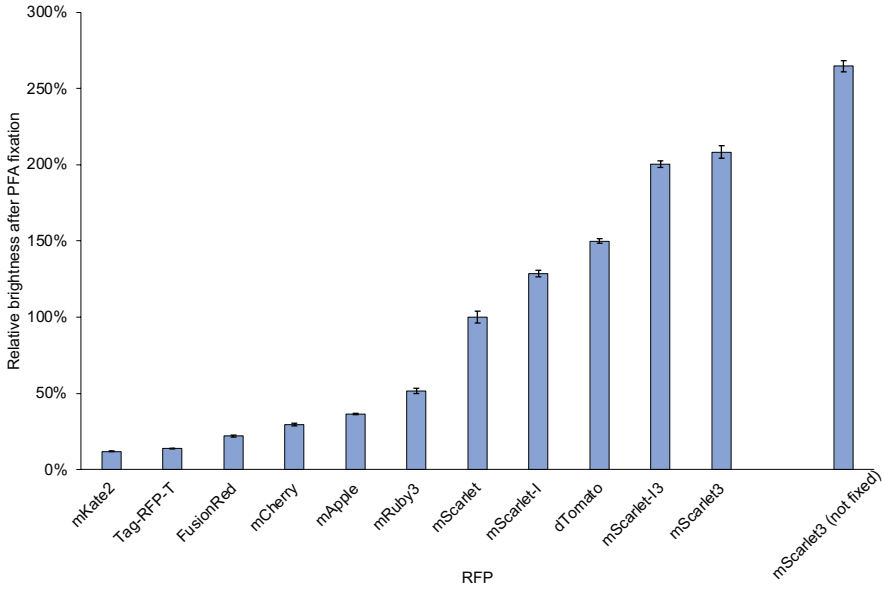
300%
250%
200%
150%
100%
50%
0%
Relative brightness after PFA fixation
mKate2
Tag-RFP-T
FusionRed
mCherry
mApple
mRuby3
mScarlet
mScarlet-I
dTomato
mScarlet-I3
mScarlet3
mScarlet3 (not fixed)
RFP

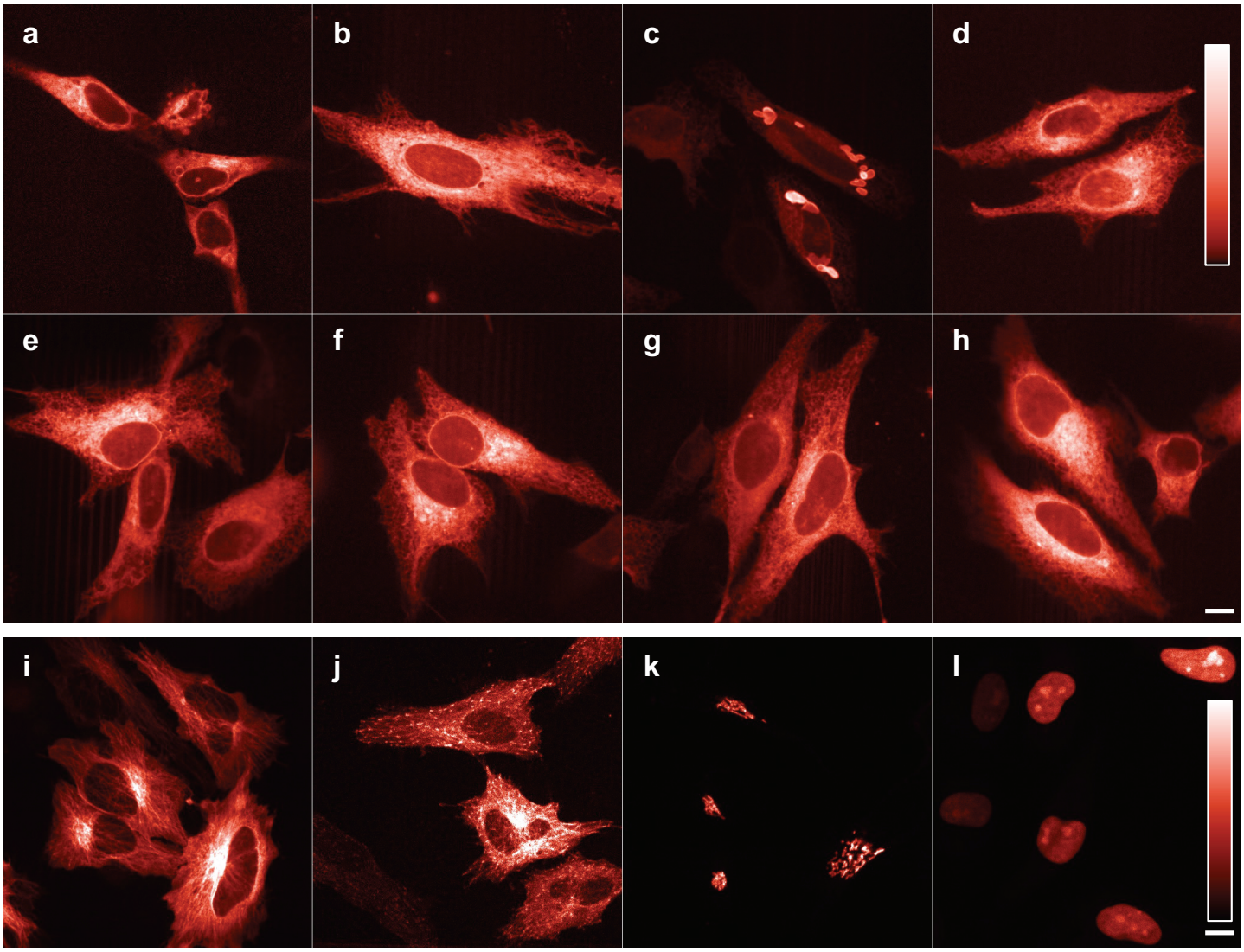
a
b
c
d
e
f
g
h

i
j
k
l

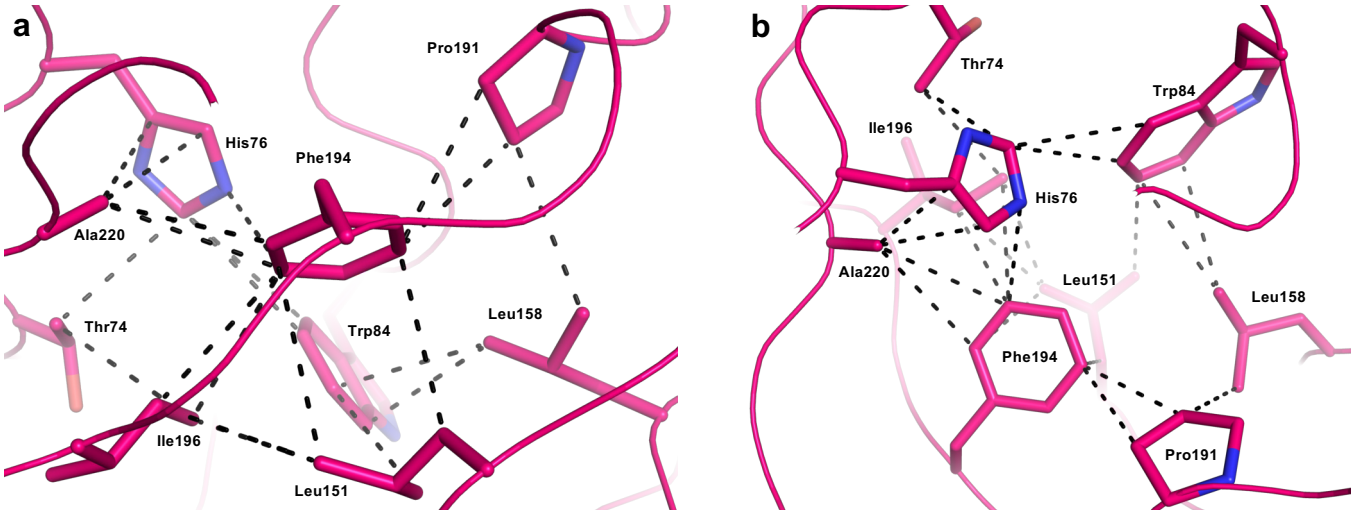
a
Pro191
His76
Phe194
Ala220
Thr74
Trp84
Leu158
Ile196
Leu151
b
Thr74
Trp84
Ile196
His76
Ala220
Leu151
Leu158
Phe194
Pro191

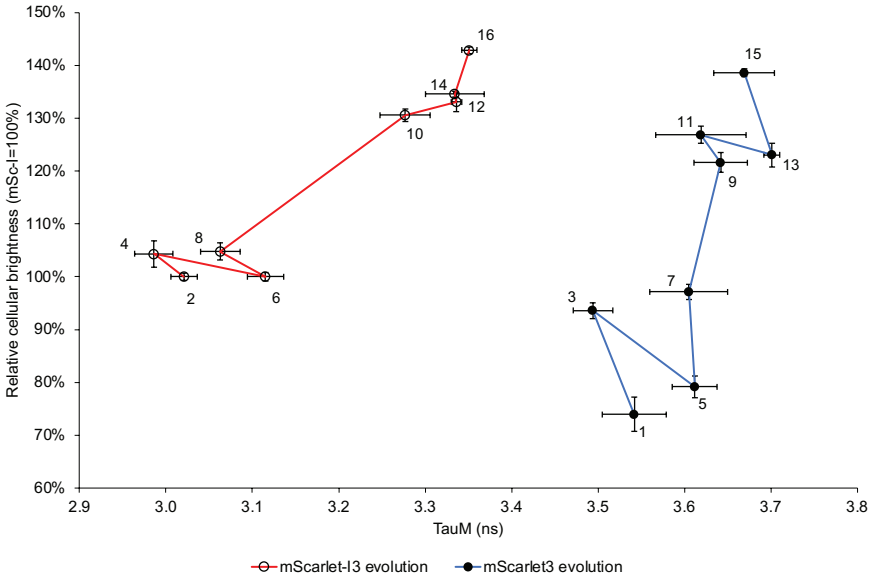
150%
140%
130%
120%
110%
100%
90%
80%
70%
60%
Relative cellular brightness (mScI-I=100%)
2.9
3.0
3.1
3.2
3.3
3.4
3.5
3.6
3.7
3.8
TauM (ns)
16
14
12
10
8
4
2
6
15
11
13
9
7
3
5
1
mScarlet-I3 evolution
mScarlet3 evolution